Stony Brook University

Characterization of Magnesium Silicide Processed with Thermal Spray

for

Thermoelectric Energy Harvesting

A Thesis Presented

by

Chao Nie

to

The Graduate School

in Partial Fulfillment of the

Requirements

for the Degree of

Master of Science

in

Mechanical Engineering

Stony Brook University

July 20

Stony Brook University

The Graduate School

Chao Nie

We, the thesis committee for the above candidate for the

Master of Science degree, hereby recommend

acceptance of this thesis.

Lei Zuo – Thesis Advisor
Assistant Professor, Mechanical Engineering

Jon Longtin – Committee Chair
Associate Professor, Mechanical Engineering

David J. Jae-Seok Hwang – Committee Member
Assistant Professor, Mechanical Engineering

This thesis is accepted by the Graduate School

Charles Taber
Interim Dean of the Graduate School

Characterization of Magnesium Silicide Processed with Thermal Spray

for

Thermoelectric Energy Harvesting

Master of Science

in

Mechanical Engineering

Stony Brook University

2013

Abstract

Mg_2Si has long been recognized as one of the promising thermoelectric materials; the fabrication methods are hot press, spark plasma sintering, high temperature sintering, etc. however, application of thermoelectric materials requires large scale manufacturing but traditional manufacturing process cannot reach this goal by its nature; thus we employed thermal spray technology to fabricate such thermoelectric material. In collaboration with Thermal Spray Center in Stony Brook University, we manufactured Mg_2Si coatings on titanium substrate by plasma thermal spray technology. Samples were further characterized in various methods: scanning electron microscopy (SEM) exhibits the micro structures of sprayed Mg_2Si coatings; X-ray spectroscopy (XRD) analysis examined the content and various thermoelectric properties by electrical conductivity measurement, thermal conductivity measurement, Seebeck Effect measurement and Hall Effect measurement. The result showed that vacuum plasma thermal spray so far has better thermoelectric properties than atmospheric plasma spray and Mg_2Si has potential to increase its thermoelectric properties if proper fabrication environment and post-fabrication processes are employed.

DEDICATION

I dedicate this work to my parents and my close friends (who are the dearest people to me in United States of America). Without their continuous support, love and encouragement, I could not achieve this.

ACKNOWLEDGEMENTS

This thesis has taken me so long to complete and so much effort to overcome the difficulties. I will never forget those people who survived me from the desperate abyss and enlightened my life so that I can complete this work.

First, I would like to express my sincere gratitude to my adviser Dr. Lei Zuo for his continuous support and guidance throughout my research. Not only did he inspire me in my research, but also his attitude to work, to academics, taught me how to peruse the life that you want. I had seen him working till late night often and his concentration and insight advice toward my lab mates' presentations in weekly meeting. He set up an example for me as how it is called "hardworking" and "passionate" to academic research. I feel deeply pleasure that I can be his student.

Next, I am very thankful for the indispensable help from my lab mate, Gaosheng Fu who is currently a Ph.D. candidate in Stony Brook University. We worked together from the beginning. He introduced me into this project and taught me the basic ideas and experiment skills. Together, we developed new methods for sample preparation, as well as improvements to our experiments. At the same time, I specially thank my committee member Professor Jon Longtin, Professor David J. Jae-Seok Hwang. They always provide me with precious help not only on the direction of our research, but also on the details of the experiment. I cannot finish all of the experiments without their help. I also want to thank Professor Sanjay Sampath and Dr. Jim Quinn from Department of Materials Science and Engineering for help in sample preparation. Their professionalism gave us significant assistance and inspired us in various ways.

I also acknowledge the financial support from NSF/DOE Thermoelectric Partnership program under grant NSF CBET #1048744 and from NYSERDA under Contract 21180.

I also would like to thank my parents for their continuous help financially and spiritually. I deeply understand that they miss me so much because I am the only child and I have not seen them for two years. I think what I can do in return is to complete my work here with effort and diligence so that their love and support me will not go in vain.

Finally I would like to thank my dear friends; some of them are also my lab mates. It is them that provide me with tasty dinner for me when I feel tired; it is them that give me rides to Flushing for cheap grocery shopping; it is them that stay with me in this office till late night so that I won't feel lonely. But above all, they gave me more than a girlfriend can do.

List of Figures

List of Tables

Content

Chapter 1

Introduction

1.1 Background

A great amount of energy is consumed by the automobile industry, in which over 40% percent of energy is wasted by the means of vehicle exhaust[1]. In order to make use of the energy that contained in the exhaust, various methods have been applied, such as mechanical turbocharger, electric turbocharger, as well as thermoelectric generator [2-4], among which the kinetic energy in the vehicle exhaust is utilized in turbocharger and heat energy is utilized in thermoelectric generator; however, turbocharger can provide driving force to vehicle by utilization of exhaust, the way that thermoelectric generator uses is to generate electricity from heat of exhaust.

Recovery of heat in exhaust is now gaining more attention nowadays. A DOE report indicates that over 350 – 390 watts of electricity can improve 3 – 4% fuel efficiency for a Chevy Suburban or a BMW sedan[5]. The key component in thermoelectric generator is thermoelectric material. The theory behind it is Seebeck effect – electricity can be generated through temperature difference. In application, temperature difference can be created via exhaust temperature and cooling part, which is water cooling.

Currently, there are various types of thermoelectric materials which are classified by operating temperature range; for example, bismuth telluride falls into low temperature range[6];

magnesium silicide and manganese silicide are intermediate temperature thermoelectric materials[7-10]; silicon germanium is high temperature thermoelectric materials[11]. Figure 1 shows the profile of common used thermoelectric materials along with ZT and temperature.

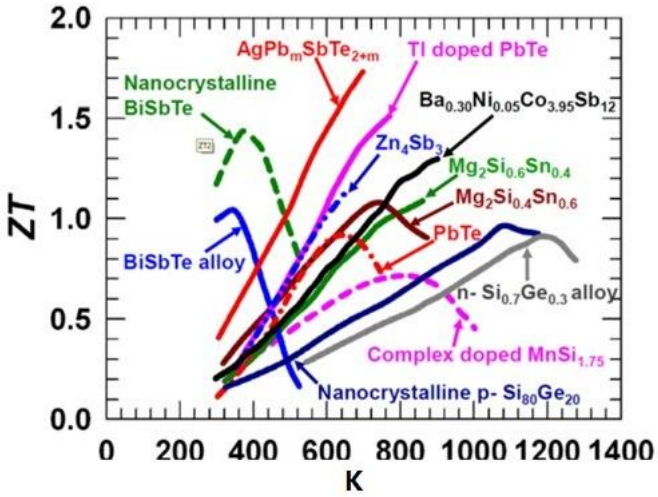

Figure 1-1. Temperature dependence of most popular TE materials[12].

1.2 Motivation

According to the vehicle exhaust temperature which ranges from 300 – 580 Celsius[13], the primary temperature range is 300 K to 800 K; therefore, the intermediate thermoelectric materials can fit this category. For lower temperature thermoelectric materials and high temperature materials, ZT (measure of thermoelectric property) is not as high as intermediate thermoelectric materials; in addition, because of the toxic nature of bismuth, lead, as well as other materials, magnesium silicide, however, is non-toxic and environmentally friendly; moreover, its abundance on earth also makes it more economic than other materials. In all, magnesium silicide falls into consideration.

Extensive research has been focused on the synthesis of magnesium silicide. Direct melting had been conducted and rendered ZT of 1.1[14]; mechanical alloying followed by hot press was investigated by Riffel and Schilz[15]; the combination of solid-state reaction and hot press was tested by Jung and Jae-Yong with ZT of 0.7 at 830 K[16]; in addition, the research from Dr. Qiang Li used melting spinning, spark plasma synthesis and hot pressing, not only demonstrated the possibility of such techniques, but also lay down the foundation that thermoelectric properties can be enhanced via non-equilibrium technique[17].

After cooperated with Dr. Qiang Li, thermal spray technology was primarily applied into fabrication of magnesium silicide. Except for thermal spray technology, the existing manufacturing methods are limited in industrial scale up and manufacturing period; thermal spray, as industry-scalable and cost-effective manufacturing process, exceeds the previous manufacturing method in these two aspects; however, thermal spray technology was originally developed for protective barrier coatings and until recently, it has been extended for fabrication of electronic materials[18].

In collaboration with Thermal Spray Center, thermal spray was applied into fabrication of magnesium silicide; however, thermal-sprayed magnesium silicide coatings had not been reported by others for the high vapor pressure and high oxidation reactivity of Mg. Therefore, developing new fabrication method and characterizing thermal-sprayed magnesium silicide became the prior goal.

1.3 Terminology

Seebeck coefficient, (also called thermo power) is a measurement of the magnitude of thermal-electric voltage responding to a temperature difference across one type of material. It is used in the description of Seebeck effect (also called thermal-electric effect), which is a direct conversion of the energy of heat that conserved by temperature differences into electric power, to generate electricity. It was discovered by the balt-German physicist Thomas Johann Seebeck in 1821.

Seebeck coefficient is represented by S. It has a unit of V/K, but μV/K is more common in use. When a temperature difference applied to a thermoelectric material, it causes the charged carriers in the material to diffuse from the hot side to the cold side. Thus the charges migrate to the cold side, leaving the positive charges, or nuclei at the hot side, creating an electric voltage (also called thermoelectric voltage) across the material. An increase in temperature difference leads to an increase in the thermoelectric voltage.

In nature, Seebeck materials are semiconductors which have p-type and n-type. P-type means a semiconductor that only has positive charges, in other word, holes; n-type of semiconductor means a semiconductor that has negative charges, i.e. electrons. Suppose that a pure p-type material is heated and Seebeck Effect happens, the temperature gradient and the electrical field are in the same direction because for p-type of semiconductor, the thermally induced mobile charges are positive, hole; and vice versa.

So the Seebeck Effect is defined as the following equation:

$$S = -\frac{\Delta V}{\Delta T} \qquad (1)$$

Note that there is a minus sign in the front of the equation. It is because the directions of the temperature gradient and the electrical field are different. To be specific, the electrical field points from the high voltage to the low voltage side while the temperature gradient is from low temperature to high temperature. So in a word, the end with high voltage has lower temperature compare to the other side.

An important dimensionless measurement for evaluating thermoelectric materials is figure of merit; it can be expressed as:

$$ZT = \frac{S^2\sigma}{k}T \qquad (2)$$

Where S is Seebeck coefficient, σ is electrical conductivity, k is thermal conductivity and T is absolute temperature. By engineering a material through Seebeck coefficient, electrical conductivity and thermal conductivity, a thermoelectric material with desired property can be achieved.

The fabricating method is thermal spray. In this study, two specific methods were used: Atmospheric Plasma Spray (APS) and Vacuum Plasma Spray (VPS). Characterization includes scanning electron microscopy (SEM), X-ray diffraction (XRD), Seebeck coefficient measurement, thermal conductivity measurement, electrical conductivity measurement and Hall Effect measurement. This thesis focuses on the characterization of materials.

1.4 Previous Literature

As mentioned above, V.K. Zaitsev and his colleagues used direct melting method to fabricate magnesium silicide. He mentioned that the increase of figure of merit of bulk materials was based on the use of lattice thermal conductivity while his work emphasized on the optimization of band structure of a solid solution. Direct melting was used in sample preparation, followed by long-time annealing in order to homogenize the structure of the sample. Based in their calculation and experiment, they confirmed that the change of nature of the states can form lower band and was favored by thermoelectricity. He also confirmed that Mg_2Si-Mg_2Sn is the one of the most promising thermoelectric material systems and the figure of merit varies with the change of its composition.

M.Riffel used mechanical alloying method to produce magnesium silicide. The advantage of such fabrication method is that it can minimize the oxidation and danger during the production. He explored the possibility of using mechanical alloying to fabricate magnesium silicide by first setting up parameters for ball milling machine; followed by examining the optimum load in 500ml vial which was found to be 10 -20 grams. The general processing time was less than 25 hours. SEM, TEM, XRD along with EDX were carried out for analyzing the powder and finally, it was proven to be feasible to use mechanical alloying.

Jae-Yong Jung and his colleagues worked on solid state reaction and mechanical alloying methods to synthesize magnesium silicide. The solid state reaction was operating at 773 K for 6 hours and the production of this reaction was doped by mechanical alloying for another 24 hours. Then the powder was fully consolidated via hot pressing for one hour at 1073K. Some properties such as electronic transport properties and thermoelectric properties were examined as

well. They proved that doped magnesium silicide exhibited great electric conductivity in that doping increased the carrier concentration; however, thermal conductivity did not changed much which was due to the much larger contribution of lattice thermal conductivity. The original figure of merit of magnesium silicide that fabricated by solid state reaction was low but it changed remarkably by doping with Group B (Bi, Sb) elements.

Qiang Li, Zhiwei Lin and Juan Zhou found that great amount of work had been focused on either bulk materials or low dimensional systems and most effort had been put into decrease of thermal conductivity. His method was to explore the means to increase power factor and to decrease thermal conductivity by nanocompositing. He demonstrated that electron correlation may be a new method to drastically increase the power factor. In addition, he used melting spinning to produce skutterudites (a type of thermoelectric material) and proved that over 30% in power factor can be achieved with this type material; moreover, melting spinning is non-equilibrium synthesis which can change amorphous materials into single-phase crystalline materials, therefore, Qiang Li and his colleague also proved that non-equilibrium synthesis can lower the lattice thermal conductivity.

1.5 Project Overview

By studying the previous literature (see table 1 above), it can be found that direct melting, mechanical alloying, solid state reaction and hot press can be applied to magnesium silicide fabrication and the novel method such as non-equilibrium synthesis; for example, melting spinning is more suitable for such fabrication. However, the disadvantages above methods are obvious: traditional manufacturing process takes relatively long time to fabricate, as well as

limited the amount of production. One of the non-equilibrium processes, thermal spray can overcome such shorts.

Eventually, the magnesium silicide based vehicle exhaust pipe energy harvesting device need to be made, the very first step is to fabricate proper materials. After theoretical modeling of optimum length for semiconductor legs, a few attempts were made to spray magnesium silicide layers on plane substrates instead of on the cylindrical pipe, in other word, 3D fabrication. Once the characterization of sprayed magnesium silicide coatings satisfy the need for energy harvesting purpose, magnesium silicide can be sprayed on cylindrical pipe and further make into a complete device that can harvest energy from vehicle exhaust.

1.6 Progress Overview and Summary

The main work of this year was to characterize the APS, VPS and hot pressed samples. The reason for including hot pressed samples was to make comparison between thermal sprayed samples and hot pressed samples. The characterization included thermal conductivity measurement, electrical conductivity measurement, Hall Effect measurement, Seebeck Effect measurement, scanning electron microscopy (SEM) and X-ray diffraction (XRD).

Different types of raw powder were used for both APS and VPS methods and for hot press method so that the influence of doping and oxidation were explored. Because of the limitation of equipment, electrical conductivity and Hall Effect were measured in Brookhaven National Laboratory and the rest characterization work was done at Stony Brook University.

During the experiment, in order to make efficient use of the sample and save time, the typical sequence of the measurements was done in the following ways: scanning electron microscopy (SEM) and X-ray diffraction (XRD) were measured in the first place and followed by the thermal conductivity, electrical conductivity, Hall Effect and Seebeck Effect.

So far, all the characterization for APS and VPS samples were finished and the result was expected, the figure of merits of APS and VPS were promising compared to hot pressed samples; at the same time, heat treatment was found helpful for improving the properties of the samples.

Chapter 2

Experiment techniques

2.1 Thermal Spray Technology

Thermal Spray had long been recognized as one of the techniques to produce surface coatings in a continuous process, in which coating material is combined with heat and kinetic energy, to form a laminate structure of droplets on substrate, where they splat, solidify and increment in vertical direction and eventually build up as a new surface.

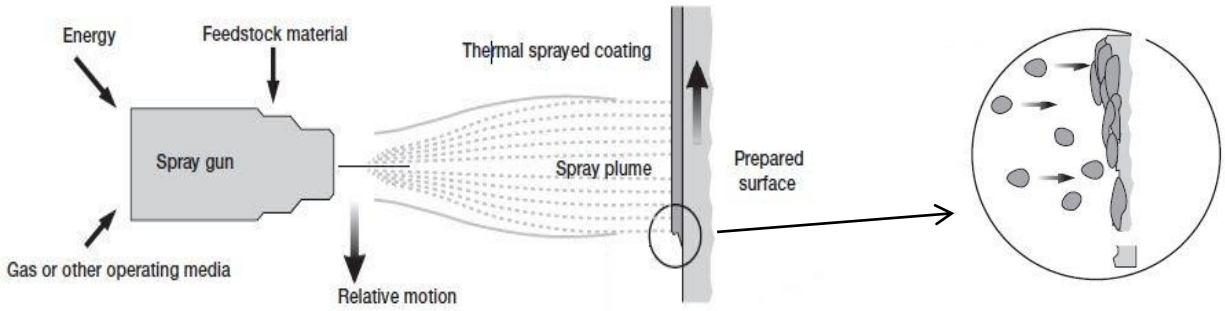

Figure 2-1. Principle of thermal spraying[19]

During the spraying, feedstock materials are heated to molten or semi-molten state and are transported by operating media, as droplets, so that the coating materials can deposit on the substrate, to accumulate vertically to form laminated coating.

Substrate materials are of great importance as well. Suitable substrate materials are those which can resist high temperature and impact from high speed droplets in the course of spraying; Substrates need to be processed before spraying since the adhesion of molten particles to the substrate is primarily mechanical bonding, instead of metallurgical bonding; thus pretreatment of substrates that to be coated is important. Surface of substrate can be cleaned by chemical or mechanical methods. Then the surface is roughened in order to provide more mechanical bonding to those molten particles and grit blasting with dry corundum is the normal way to roughen the surface.

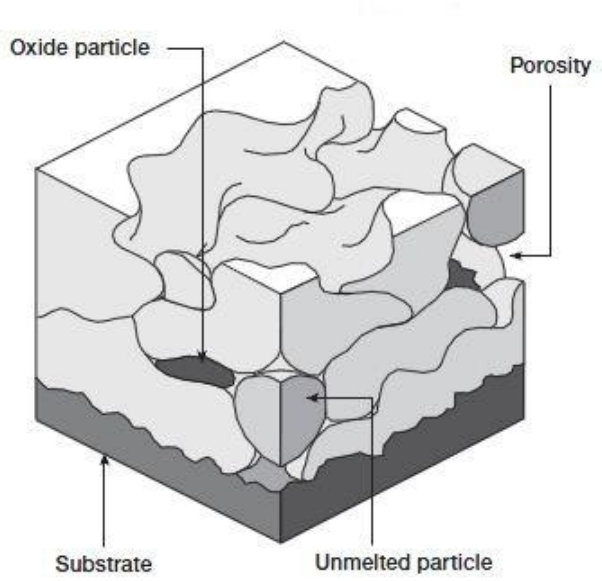

Figure 2-2. Illustration of thermal sprayed coatings[19]

Since the molten particles hit the surface at high speed, they usually deform after hitting the surface. For those particles that are not melted during the spray, they will stay in the coating as the splats accumulate around, the un-melted particles will be buried inside the coating. Hot particles will shrink and solidify, forming a mechanical bond dominated structure; metallurgical bond happens during the diffusion between particles and substrate and particle to particle, but such bonding mechanism is so small to be neglected.

Thermal spray processes can be classified into conventional flame spray, electric arc wire spray, plasma spray and high velocity oxy fuel spray[19].

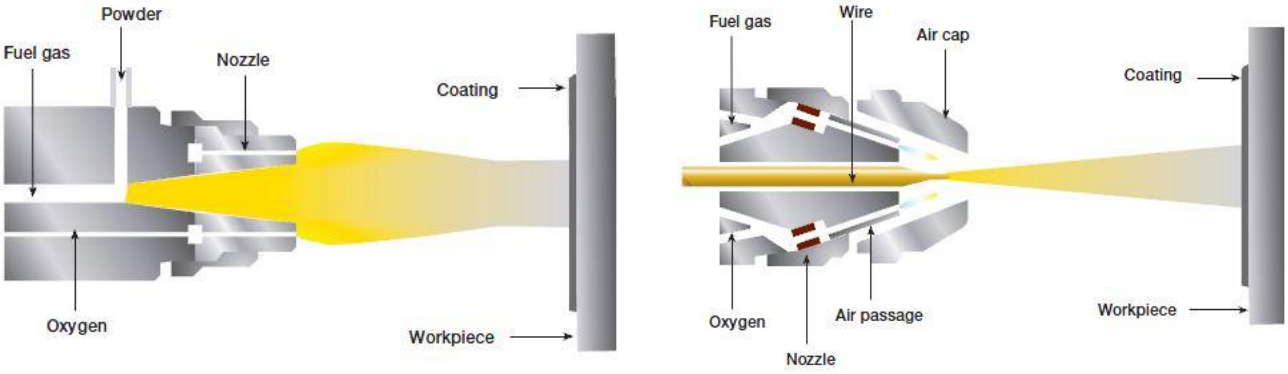

Figure 2-3. (a) Diagram of powder flame spray; (b) diagram of wire flame spray

Both powder flame spray and wire flame spray (Fig 2-3a and Fig 2-3b) belong to conventional flame spray process. Powder or wire is melted in the flame of gaseous fuel, such as acetylene, propane or hydrogen. Once the feed material is melted, the compressed air can carry the melted and atomized toward the substrate to form layered structure. Not all the materials can be fabricated into wire, the powder flame spray expand the materials selection for thermal spray.

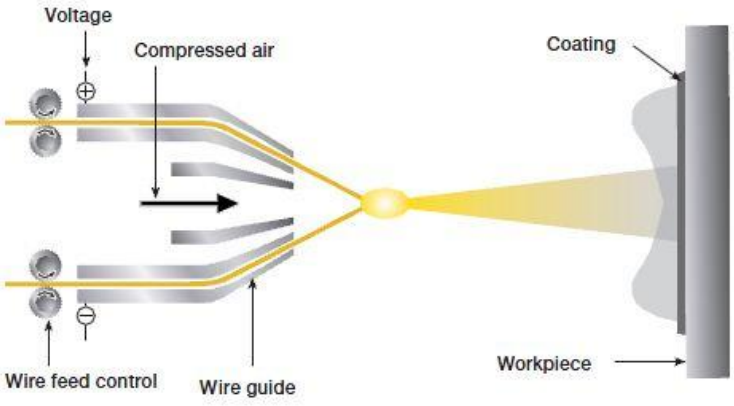

Figure 2-4. Diagram of electric arc wire spray

Different from flame spray, electric are wire spray applied opposite charge to the two wires (shown in Fig 2-4), the contact of these two wires can trigger the melt of the tip; compressed air is then blew into, to take the melted part to the substrate. Appropriate control of wire feed speed regulates the melt at a constant speed.

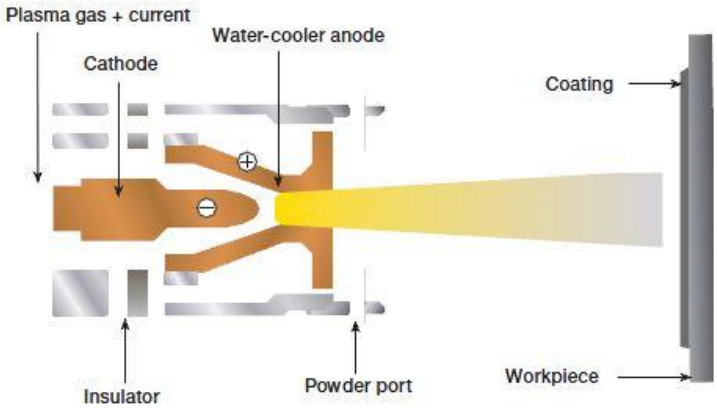

Figure 2-5. Diagram of plasma spray

The principal of plasma spray is based on the formation of high temperature plasma. The gas, such as helium, hydrogen, nitrogen or mixtures, flow though the cathode and anode, which are charged by high frequency current, is being ignited by the arc between these electrodes to form plasma plume; coating material is fed outside and is carried by the plasma plume onto the substrate. Since the temperature can reach as high as 16000K, the injected powder can be melted before they reach the substrate. According to special applications, plasma spray varies from atmospheric plasma spray (APS) and vacuum plasma spray (VPS). One significant advantage of VPS is its low oxidation rate but it requires higher energy input to melt the particles than APS.

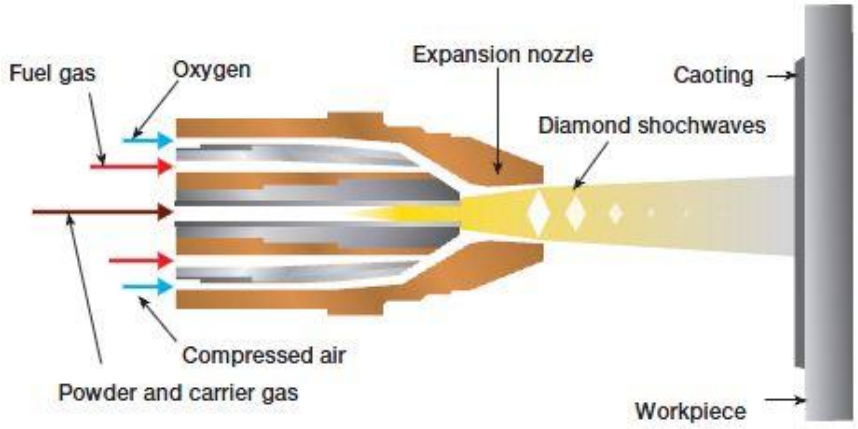

Figure 2-6. Diagram of high velocity oxy-fuel spray

High velocity oxy-fuel spray (HVOF) is new to the family of thermal spray processes. It differs from other processes is that it used supersonic air flow jet to carry the melted particles. Fuel gas and compressed air are injected as shown in Fig 2-6. The impact of particles on the substrate is much higher than flame spray which can result more dense coating.

Even though all the processes can form laminate structure, the density of such structure varies according to different types of spray. HVOF has much higher kinetic energy than other spray process, thus it can result in much denser structure with nearly 0.5% porosity and plasma spray, since it has much higher thermal energy but relatively low kinetic energy, usually it can produce layers with 1-2% percent porosity and to be specific, controlled APS can produce fully dense laminate structure.

During operation, the thermal spray gun travels back and forth over the surface, each time as the gun travels, it can produce a layer of coating with 10 – 20 micrometer thickness. Oxidation happens at this time and melting process. Therefore, oxides can be found in the cross section of the layer. In application, depending on the requirement of the objective, oxidation can be

minimized or neglected. The typical way to avoid oxidation is to use VPS; however, VPA cannot achieve zero oxidation percent.

The contamination can be found from 3 sources: raw powder, spray gun and substrate. As mentioned before, the contamination on the substrate can result weak mechanical bonding between coating and substrate. In the coating, contamination, or, impurities may from raw materials or thermal spray gun. Impurities can be trapped in the coatings as the spraying process continues. This can lower the stress of the coating and affect the properties of the coatings. In some cases, impurities can improve the properties but it depends on the purpose of spray.

Post-coat treatment is necessary since the surface of thermal sprayed coating is rough and internal cracks and porosity can affect the mechanical properties, as well we thermal conductivity and electrical conductivity. Polishing and heat treatment are the typical treatment that applied on the coatings. In other word, polishing can smooth the surface in wear protection application and heat treatment can decrease the amount of cracks and porosity.

2.2 Materials characterization

In this project, the following material properties need to be measured: thermal conductivity, electrical conductivity, Seebeck Coefficient, Hall Effect measurement and SEM & XRD analysis. According to the equation of ZT, shown as follow:

$$ZT = \frac{S^2\sigma}{k}T$$

S represents Seebeck Coefficient, σ represents electrical conductivity and k represents thermal conductivity.

2.2.1 Thermal conductivity measurement

In this project, the instrument that is used for measuring thermal conductivity is from TA Instruments. The thermal conductivity is defined as:

$$k = \frac{Q/A}{\Delta T/\Delta L} \qquad (3)$$

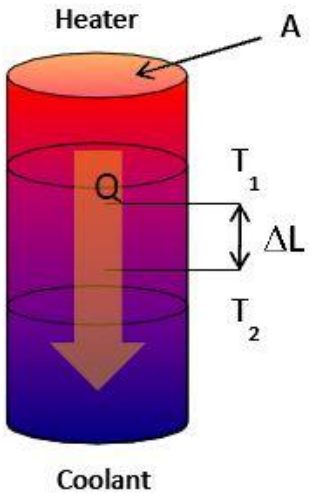

Figure 2-7. Heat transfer across the specimen[20]

Where Q is heat input, A is the area of the cross section of the specimen, ΔT is temperature difference and ΔL is the distance between these two temperatures (Fig 2-7). The combination of temperature difference and distance can create a heat flux; the measurement of thermal conductivity is always related to the measurement of the heat flux. The difficulties of this measurement lay on the measurement of heat flux. Currently, there are two methods for

measuring heat flux: absolute and comparative methods. The “absolute” refers to measurement of electric power though the heater and certain distance; “comparative” means measurement from comparison. The heat flux must be uniaxial through the sample so that the heat loss during the measurement can be minimized.

In the measurement, the thermal conductivity of the sample itself affects the measurement. If the thermal conductivity is high, such as metal, the specimen is usually made into the form of cylinder and it is easier to generate the temperature gradient along the uniaxial direction after the heat is introduced; thus it is easier to measure the heat flux. One thing need to be concerned is that the heat loss from the lateral surface. Compared to the heat transfer along the specimen, the heat loss from the lateral surface is relatively small for long cylindrical specimen. Therefore, the measurement can achieve high accuracy. Speaking of low thermal conductivity specimen, the specimen is usually made into small disk or plate because there is relative low heat flux along the sample, in order to make accurate measurement, the heat loss from the lateral surface affects the measurement more than large specimen; thus lower the length of the specimen, by making it into disk, can reduce the lateral surface area in order to decrease the heat loss from it. However, in high temperature measurement, the heat loss from the lateral surface is allowed to be high and is accounted quantitatively in the thermal conductivity measurement.

For axial flow method, it has long been recognized as the one of the most stable and accurate measurement at cryogenic temperature. One main concern in this measurement is the minimization of heat loss in radial direction as the heat is transferred along the axial direction. The heat loss is small at low temperature range but it can be great contributor for error at high temperature and, in addition, the control of heat is becoming more and more difficult in high

temperature range. Therefore, great attention has been focused on the minimization of effective conductance of specimen to lateral insulation conductance.

Several methods of thermal conductivity are listed below:

ASTM E1225 Test method is also called comparative cut bar, which is most widely used method for axial thermal conductivity measurement. In this method, heat flux passes through both a known sample and an unknown sample and the comparison can be made from thermal gradient which is inversely proportional to their thermal conductivities. The known sample is called reference. Usually the unknown sample is inserted between two known samples; by using the equation listed below, the thermal conductivity can be calculated:

$$\frac{Q}{A} = K_S \frac{\Delta T_S}{L} = K_R \frac{\frac{\Delta T_1 + \Delta T_2}{2}}{L} \frac{1}{L} \qquad (4)$$

Where K_R is the thermal conductivity of the reference and K_S is the thermal conductivity of the unknown sample; the rest are shown in the figure below.

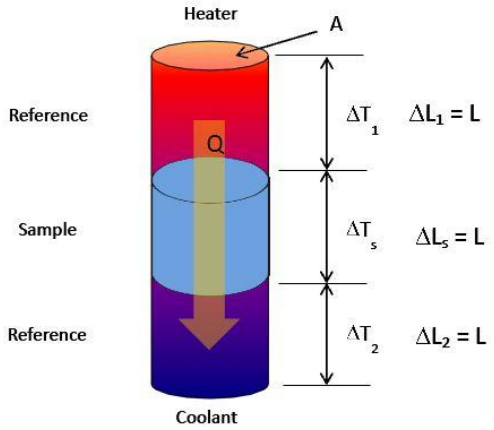

Figure 2-8. ASTEM 1225 test method illustration [20]

The thermal conductivity testing machine that we used in the project is in the following picture:

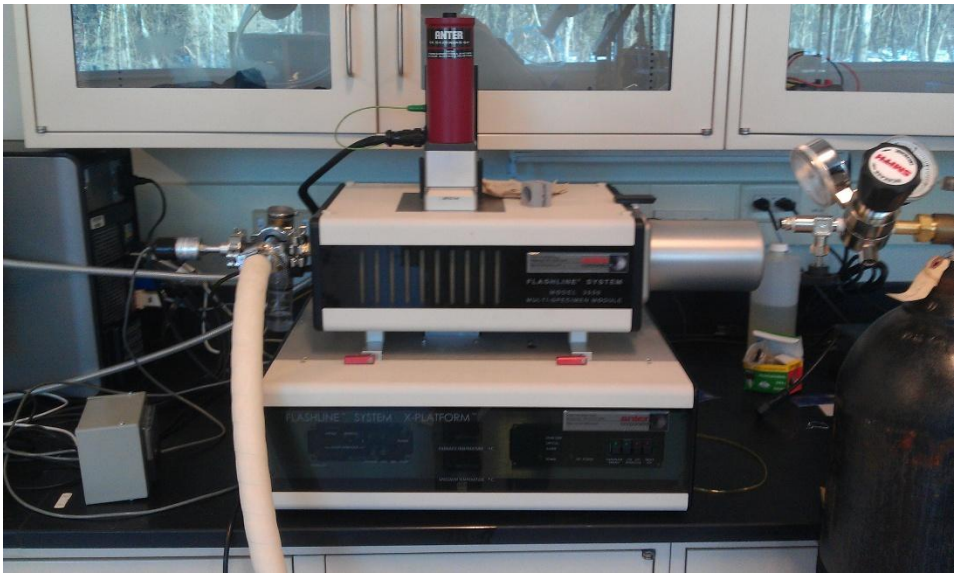

Figure 2-9. Thermal conductivity testing machine part view

Figure 2-10. Thermal conductivity testing machine whole view

The red cylinder on the top of the machine is used for liquid nitrogen container, which is used for cooling purposes during the experiment. Remember that laser flash will be flashed during the experiment, liquid nitrogen can be used as proper cooling material because 1) it has low temperature 2) it evaporates only be become gaseous nitrogen which is not being viewed as contamination. A vacuum pump is

connected to the testing chamber and the testing chamber has to be vacuumed every time before start to run. After vacuum the chamber, the nitrogen tank, which is the black tank on the right hand side of the picture needs to be turn on so that the testing chamber can be filled with nitrogen as protection gas. At the same time, there is water cooling system in the machine so that the testing chamber can be cooled when needed and at the same time, protect the machine from overheating.

2.2.2 Electrical conductivity measurement

The measurement of electrical conductivity is based on the flowing three equations:

$$R = \frac{V}{I} \qquad (5)$$

$$\rho = R\frac{A}{L} \qquad (6)$$

$$\sigma = \frac{1}{\rho} \qquad (7)$$

The first equation is Ohm's law; R is electrical resistance, V is voltage across the measured sample and "I" is the current that flows through the sample. The unit of R is Ohm, Ω. The second equation is Pouillet's law; ρ is electrical resistivity, R is electrical resistance, A is the area of the cross section of the specimen and L the length of the specimen; electrical resistivity has a unit of ohm•meter, Ω•m. The third equation is the definition of electrical conductivity; electrical conductivity is expressed as σ, it is inversely proportional to electrical resistivity. It has an SI unit of Siemen per meter (S/m).

Electrical resistivity can be measured by “two probe method” and “four probe method”, and electrical conductivity can be calculated according the third equation above.

For a long and wire-like specimen with uniform structure and composition, or a sample of parallelepiped shape with uniform structure and composition, the electrical resistivity can be measured by applying an electrical current across the specimen and measure the electrical voltage at the two ends of the specimen. Combining equation (5) and (6), the electrical resistivity can be written as:

$$\rho = \frac{V}{I}\frac{A}{L} \qquad (8)$$

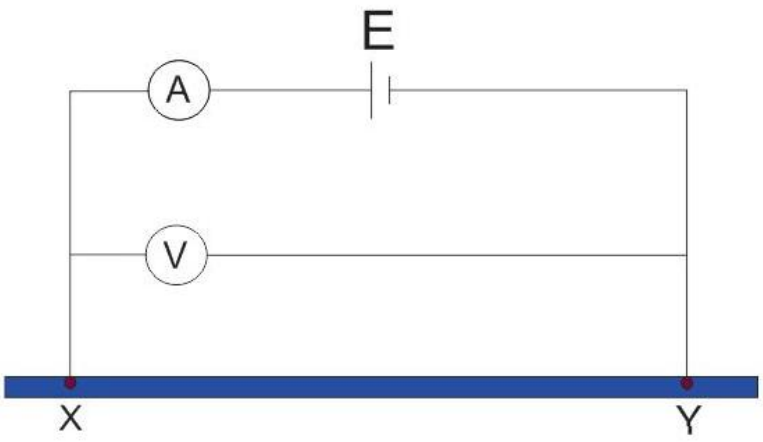

Figure 2-11. Two-probe method

All the measurement can be completed by using multi-meter. The two probe can be placed at X and Y positions to apply current. The blue bar is the specimen that is to be measured.

However, there are limitations about two-probe method: the contact between two probe and specimen can be the reason of error; this method can only measure wire-like sample and at the same time, if the wire is too thin, it will be more difficult to contact the two probes; In

addition, two probe is not as accurate as four probe because in four probe method, the voltage meter have large impedance.

Four-probe method eliminates the limitations of two-probe method. It can measure sample with various shapes. The typical set up of this method is equal-distance placement of four in-line probes, or points, the spacing of between every two probes is usually 1 mm. Current is applied through the outer two probes and is measured; at the same time, the inner two probes measure the electrical voltage between these two points and then calculate the electrical resistivity.

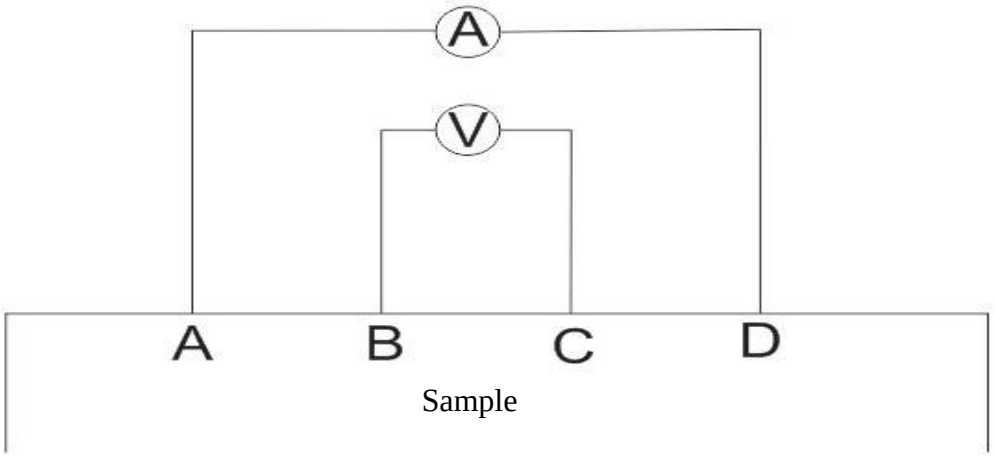

Figure 2-12.Four-probe method

As shown in the fig 11, A and D are the outer probes which apply and measure the current through the sample; B and C are the inner probes which measure the voltage. One thing need to be noted is that the surface condition is very sensitive to the measurement because contaminations, such the oxidation of the surface can contribute increase of resistivity or, affect the contact between the probes and sample.

When measuring resistivity of a large specimen, the equation of the electrical resistivity can be written as follow[21]:

$$\rho = \frac{V}{I} 2\pi s \qquad (9)$$

It is assumed that the thickness of the sample is larger than the distance between every two probes; usually it is five times larger; here, s stands for the distance between every two probes.

In this project, electrical conductivity usually takes place at a conducting substrate or non-conducting substrate. The equations for these conditions are:

$$\rho = \frac{\rho_0}{G_6(t/s)} \qquad (10)$$

$$\rho = \frac{\rho_0}{G_7(t/s)} \qquad (11)$$

In these two cases, ρ_0 stands for the electrical resistivity of large specimen. The denominators of the two equations are value of functions which can be found in the literature. When the ratio of thickness over distance is small, they can be replaced by such formula:

$$G_7(t/s) = \frac{2s}{t} ln2 \qquad (12)$$

Insert equation (12) into (11), the electrical conductivity can be written as:

$$\rho = \frac{\pi t}{ln2} \frac{V}{I} = 4.5324 \cdot t \cdot \frac{V}{I} \qquad (13)$$

In order to get more precise data, finite thickness correction f_1 and finite width correction f_2 are added behind. Both these parameters can be calculated:

$$f_1 = f_{11}(t/s) \qquad (14)$$

$$f_{11} = \frac{ln2}{ln\left[\frac{\sinh(t/s)}{\sinh(t/2s)}\right]} \qquad (15)$$

Equation (14) and (15) are for a non-conducting substrate.

$$f_1 = f_{12}(t/s) \qquad (16)$$

$$f_{12} = \frac{ln2}{ln\left[\frac{\cosh(t/s)}{\cosh(t/2s)}\right]} \qquad (17)$$

Equation (16) and (17) are for a conducting substrate. They can be simplified as two situations, shown as follow:

$$t \ll s, \quad \rho = \frac{8\pi}{3}\frac{s^2}{t}\frac{V}{I}f_2$$

$$t \gg s, \quad \rho = 2\pi \cdot s\frac{V}{I}f_2$$

f_2 dominates the equations and it can be expressed as:

I. $f_2 = f_{2c}$ (d/s), this is for a circular sample with a diameter of d.

II. $f_2 = f_{2R}$ (a/d, d/s), this is for a rectangular sample; a and d are width and length.

Meanwhile, all the parameter can also be found in the literature[22].

2.2.3 Seebeck Coefficient measurement

The measurement of Seebeck Coefficient is always difficult to achieve because this measurement is based on the electrical voltage respond and temperature difference across the sample. Usually the unit of electrical voltage is micro volt which is so small that can be easily affected by the noise. In this project, the equipment for measuring Seebeck Coefficient is from MMR Technologies, see the pictures below:

Figure 2-13. Seebeck testing machine front view

Figure 2-14. Seebeck testing machine top view

As introduced above, the Seebeck coefficient relates to temperature difference and is a response to the thermoelectric voltage. Therefore, it can be defined as follow:

$$\mathrm{S} = -\frac{\Delta V}{\Delta T}$$

Where, ΔV and ΔT are voltage difference and temperature difference.

According to this equation, the value of S can be deduced. One way to calculate Seebeck from MMR technology[23] is as follow:

$$V_1 = S_1 \times \Delta T \qquad (18)$$

$$V_2 = S_2 \times \Delta T \qquad (19)$$

Where, the subscripts 1 and 2 represent sample and reference. Both these two materials have same temperature difference, thus:

$$S_1 = S_2 \times \frac{V_1}{V_2} \qquad (20)$$

Note that the temperature difference is small, so is the thermoelectric voltage, any noise could affect the result of the measurement and such noise can hardly be removed since they may come from small parts in the measuring equipment, such as wires, connectors. Thus the direct measurement will not render high accuracy; however, the accuracy can be improved by taking two different measurements, using different sets of power parameter. The equation can be expressed as follow:

$$V_1(P_1) = S_1 \times \Delta T(P_1) + \Delta V_1 \qquad (21)$$

$$V_2(P_1) = S_2 \times \Delta T(P_1) + \Delta V_2 \qquad (22)$$

Where ΔV_1 and ΔV_2 are the undesired thermoelectric voltages, called offset voltage, produced by the equipment; P_1 is the power that applied to the heater at the first time. The other set of measurement can be expressed as:

$$V_1(P_2) = S_1 \times \Delta T(P_2) + \Delta V_1 \qquad (23)$$

$$V_2(P_2) = S_2 \times \Delta T(P_2) + \Delta V_2 \qquad (24)$$

The offset voltages can be assumed to be the same because these offset voltages are caused by the dissipated heat from the heater; the immediate power change in the heater will only affect the sample and reference area. Based on the combination of equations (21) to (24), the overall value of Seebeck coefficient can be obtained:

$$S_1 = S_2 \frac{\{V_1(P_1) - V_1(P_2)\}}{\{V_2(P_1) - V_2(P_2)\}}$$

In order to acquire accurate data during the measurement, the temperature control is of key importance. MMR Technologies uses a secondary heating process to eliminate such noise.

During the measurement, the calculation is based on the temperature difference across the sample; however, such temperature difference is not generated by the heater located below the sample but from the resistor in the front of the sample (See Fig 2-15 and Fig 2-16). For example, from temperature range 300K to 350K, the first heater brings up the temperature of the sample and reference to 350K and at this time, the secondary heater gives out the power to the sample and reference to heat up the sample so that a temperature difference can be generated, which is normally ranges from 1 – 3K, which is based on the different materials and power input.

Samples for Seebeck measurement were polished before testing. Sample size should be no longer than 4 mm in length and the diameter should be 0.7 mm. In fact, the coatings were hard to make into cylinder shape; so during the experiment, sample was made into rectangular shape with each size of short length 0.5-0.7mm and 4mm in length. Since the polishing techniques were exactly same as polishing the substrate, the glue had to be used. Once the polishing was done, the glue needed to be washed off by actone completely otherwise, it would affect the result of the measurement. Remember that the Seebeck Coefficient measurement requires a sample and a reference material, which is constantant wire. The thickest wire was around 0.7 in diameter so that the only thing that need to be done was to cut the wire into the same length as the sample.

The sample and reference material were place on the thermal stage in V shape as discussed before with silver paste applied as glue. Note that the silver paste needed to be pasted on the stages several times, to create several layers of thick paste before put the samples on it because the the single layer of silver paste would be too thin to create solid bond. As the same time, the resistance of the black resistor that located on the top of the thermal stage needed to be checked, the value should be 100 ohms. After the silver paste was complete dry, the thermal stage can be put into the vacuum chamber to start the test.

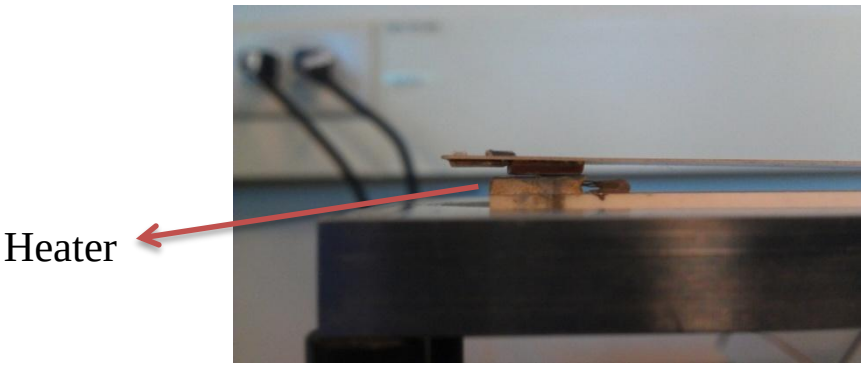

Figure 2-15. Lateral view of sample mounting

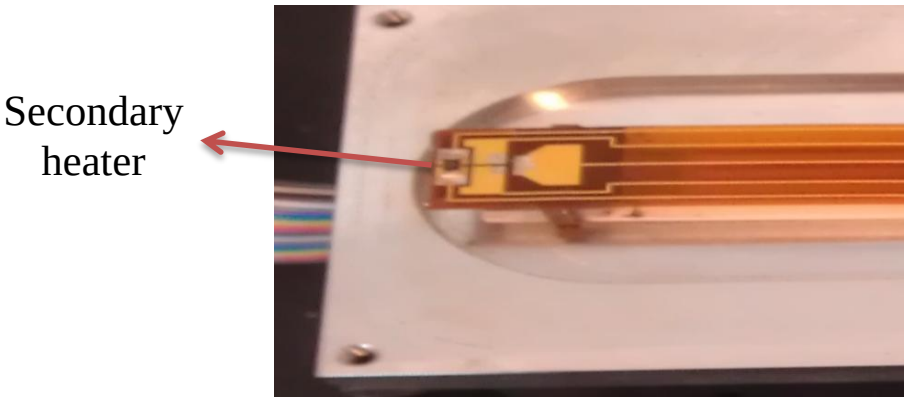

Figure 2-16. Top view of sample mounting

The heater in the vacuum chamber is called “refrigerator” because the primarily purpose of it was to cool down but here, it worked as heater (see Fig 2-15). It could go up to 730 K. In

order to have a reliable heat transfer between the heater and the thermal stage, thermal paste should be put in between. Reliable thermal paste should be dense because the bottom of the thermal stage may not be flat and so that dense thermal paste can fill up the dent of the thermal stage and last till the end of the test. This was extremely helpful when using the ceramic thermal stage.

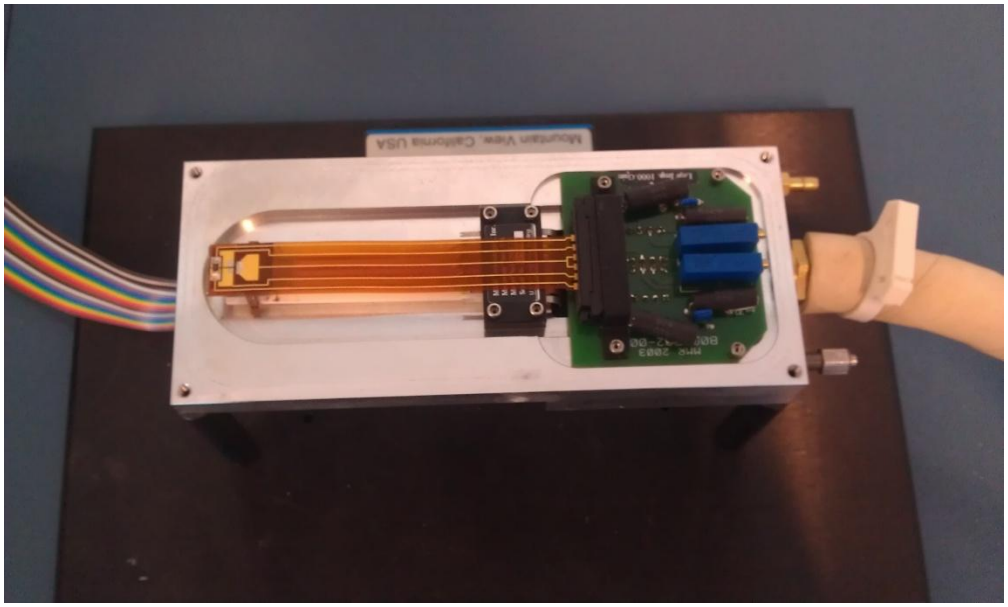

Figure 2-17. Seebeck testing machine vacuum chamber

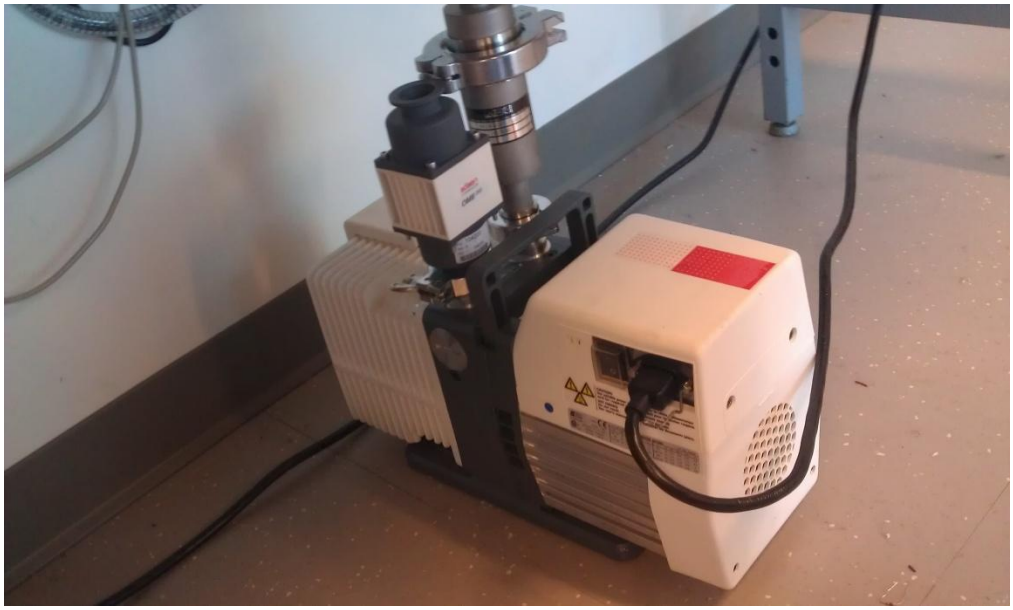

Figure 2-18. Seebeck testing mahine vacuum pump

After inserting the thermal stage in the vacuum chamber, put the vacuum cover back on and start vacuuming the chamber, see Fig 2-17 and Fig 2-18 above, that is the vacuum pump which can vacuum the vacuum chamber. The desired pressure inside would be below 100 mTorr but during the experiement, it went down to around 20-30 mTorr. Turn on the pump, the pressure gauge can read the pressure inside the chamber. At the same time, the machine needed to be warm up; To be specific, double click the icon of K-20 on the desktop of the computer, and then check the connection between the computer and the machine; click “test” botton in the software, then click “TS” botton to check the sensor type, if it tell you the tyoe of the sensor, which should be RTD256, it means the sensor works fine. Then to check the connection, by clicking “TE”, if the connection is good, it should tell you the current temperature; if neither of them works, or just one of the does not work, try restart the software, if it cannot solve the problem, disconnet all the ports and re-connect them after 5 seconds, and follow the same procedure to test the machine. if everything was ok, click “start” to start monitoring the temperature and then set up the destine

temperature. In the experiment, the starting temperature was usually around 300K and the destine temperature for heating up was 302-303K, or any temperature that below your exprimenting temperature. The whole warming process takes 10 min. It would be better warm the machine every time before start the test.

After 10 minnutes warming up, turn off the K-20 software and double click the SB-100 icon to start control the Seebeck testing machine. Same as using the K-20 software, check the connection before start using the machine; the first that need to be checked was connection. “TC” can tell the connection, if the software says “communication is OK”, it means you can go the next step; if not, restart software or disconnect and re-connect the ports. Then click “TE”, it should check the sensor and tells the temperature now which should be the destine temperature; then the check the voltage of the sample and reference. “GV1” can tell you the voltage of the reference and “GV2” tells you the voltage of the sample. Both of the votalges should be within the plus or minus 100 μV but the standard that was used during the experitment was aroung plus or minus 50 μV. At this time, if the voltage is not within this range, the mearument should be terminated because it would not give accurate measurement; One of the typical reson the caused this was bad sample mounting; if the voltage is ok, the measurement can begine.

Click the setting menu and set the starting temperature and final temperature, and temperature step as well. The operationg delay and initial delay were used default, 30 sec for each of them; the power input varies, 60 mW for Kapton thermal stage, 130 for ceramic thermal atage. After setting up the parameters, click “play” botton in the software. The way to check if the measurement is correct was to check the temperature difference. The correct one should be above 1K, if not, check out improving the power input, if nothing changes, that means the sample mounting was not good enough; or, check out the fuse on the back of machine; note that

the incorrect resistance of the black resistor that located on the top of the stage can cause the short of the fuse. As the temperature goes up, the Seebeck Coefficient should change along with it; if not, it could because of the bad heat transfer between the heat and thermal stage; or because of the bad sample mounting.

2.2.4 Scanning electron microscopy (SEM) and X-ray diffraction (XRD) analysis

SEM refers to scanning electron microscope. The principle of scanning electron miscopy is that the electron gun generates an electron beam and this beam will hit the surface of the specimen through a vacuum column; then the electrons will interact with the surface region or even in a depth of approximately 1 micrometer and generates signals to form image. The other feature of scanning electron miscopy is EDS, energy dispersive spectrometer. It can render the map of elements in a certain area.

XRD is X-ray diffraction. Since many materials have crystal structure, semiconductor is one of them; it is one of the fundamental characterization skills. Not only can X-ray diffraction tell the atomic structure of a certain type of material but also the composition of the material.

Chapter 3

Experiment Summary

3.1 Atmospheric Plasma Spray (APS)

Raw magnesium silicide powder with 98% purity was purchased from YHL, New Energy. Co.Ltd (Zhejiang, China). The particle size ranges from 25 micrometers to 270 micrometers. Proper particle sizes were needed in the thermal spray process since overly large or small particles would clog the thermal spray torch so that powder should be sieved before using. According to the requirement of thermal spray, powder with 53 to 180 micrometers sizes were used as feedstock powder. High purity powder was expected, however, high purity and desired particle sizes could not be reached at the same time. A 40 kW plasma spray system (Miller Thermal, USA) was used as deposition method.

Thermal spray coatings were deposited on pre-heated aluminum/ titanium substrate with the size of 40 $\times$25 $\times$2 mm. For most of the measurement, substrate was not necessary, such as electrical conductivity measurement, thermal conductivity measurement, Seebeck Coefficient measurement; in addition, annealing could not be carried out with aluminum substrate since the melting temperature of aluminum is 660 degree C and the typical annealing temperature that had been used was 750 degree C or less; therefore, substrates were peeled off by polisher with sand paper of rotating speed at 60 -120 ppm.

Furthermore, in the thermal conductivity measurement, the sample has to be cut into circle with half inch diameter and polished to 0.04 inch in thickness; electrical conductivity measurement can be done in various dimensions, the one that had been typically used was 10 × 2 × 1mm and the surfaces of the sample were polished with sand paper from 320 mesh to 800 mesh because the roughness of the surface can greatly affects the contact of wires to the surface even though silver paste was applied as connection between wires and surface; Seebeck Coefficient samples were made into small dimensions: 4 × 1 × 1mm with polisher. Scanning electron miscopy samples were also polished up to 0.5 micrometer polishing disk before test.

3.1.1 SEM Images and XRD analysis of APS and Hot Pressed samples

In the beginning of coating fabrication, powder was used for making thermal spray splats in order to make an understanding of quality of the powder. Scanning electron miscopy images were shown below:

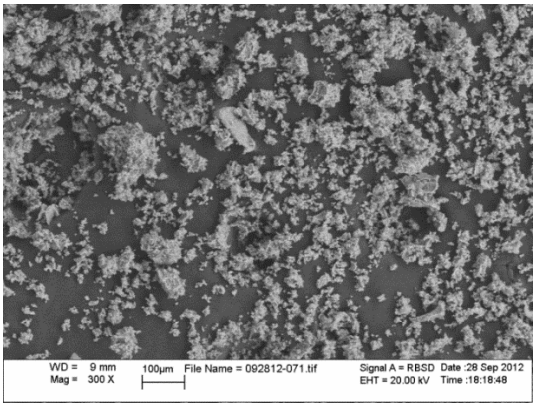

Figure 3-1. Raw Mg_2Si powder for thermal spray

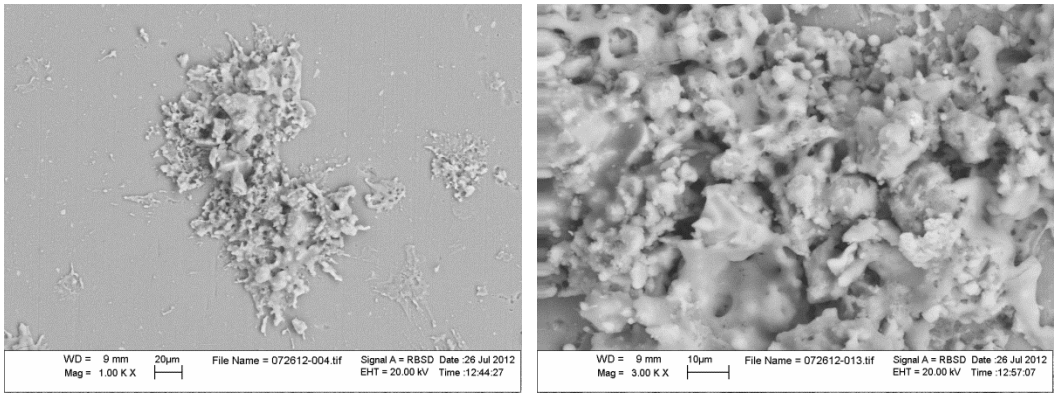

Figure 3-2. Thermal spray splat of Mg_2Si and 3000kX magnification

Figure 3-1 shows the shapes of raw powder. This powder deviates from high quality thermal spray powder because the shape of this type of powder doesn't have unified round shape and this can affect the flowability of powder. Figure 3-2 is magnesium silicide splat with same powder. It can be easily seen that the powder particle was melt but the splat was in porous structure. Figure 3-3 is the magnification of same splat with 3,000 magnification rate in order to examine the composition of such splat.

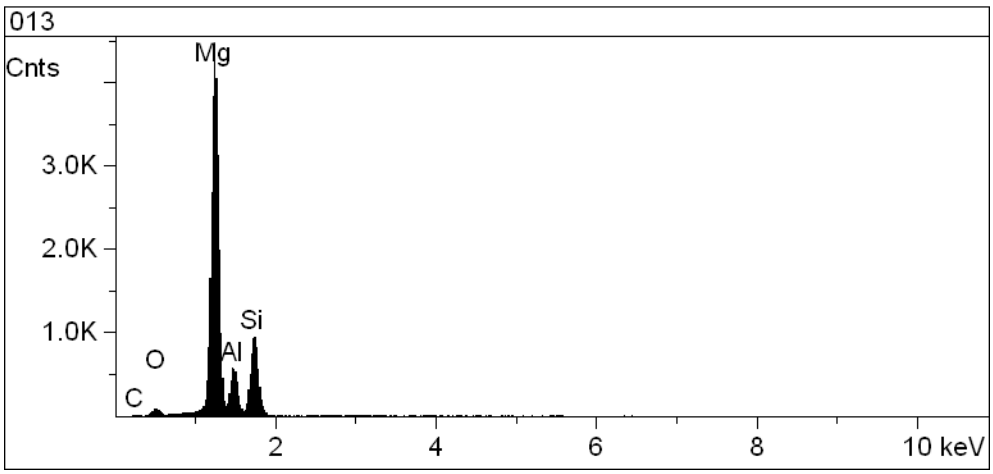

Figure 3-3. EDS image of Mg_2Si splat

From figure 3-3, it is clearly shows that the composition of such splat was magnesium silicide with impurities of aluminum, carbon and oxygen.

In the later experiments, a thin layer coating (300 micrometers in thickness) was made with such powder. Since this is atmospheric plasma spray, magnesium silicide can react with oxygen in the air to form magnesium oxidize and silicon and this reaction is easy to happen according to the formula:

$$Mg_2Si + O_2 \xrightarrow{450℃} \mathrm{MgO} + \mathrm{Si}$$

Multiple techniques were used to prevent the oxidation of powder during the spray such as application of shroud in the APS torch (sample R2018), switch into smaller nozzle (sample R2096) and switch of torch (B006). The parameters are listed below:

Table 3-1. Parameters of APS

Sample	Temperature(℃)	Velocity(m/s)	Torch type
R1961	1781	155	8mm nozzle
R1962	1834	183	8mm nozzle
R2018	1850	155	8 mm nozzle, shroud
R2069	1820	232	6 mm nozzle
B006	Low	High	SG100

In detail, sample R1961 and R1962 were used with same nozzle but different temperature and velocity in order to compare the influence of temperature and velocity on thermoelectric properties; R2018 was sprayed with a shroud so that the oxidation rate can be found with comparison of R1962 or R1961. As sample B006, SG100 torch was used to make coating so that different oxidation rate can be found. Same to R2096, examination can be made to find out the oxidation rate with application of small nozzle.

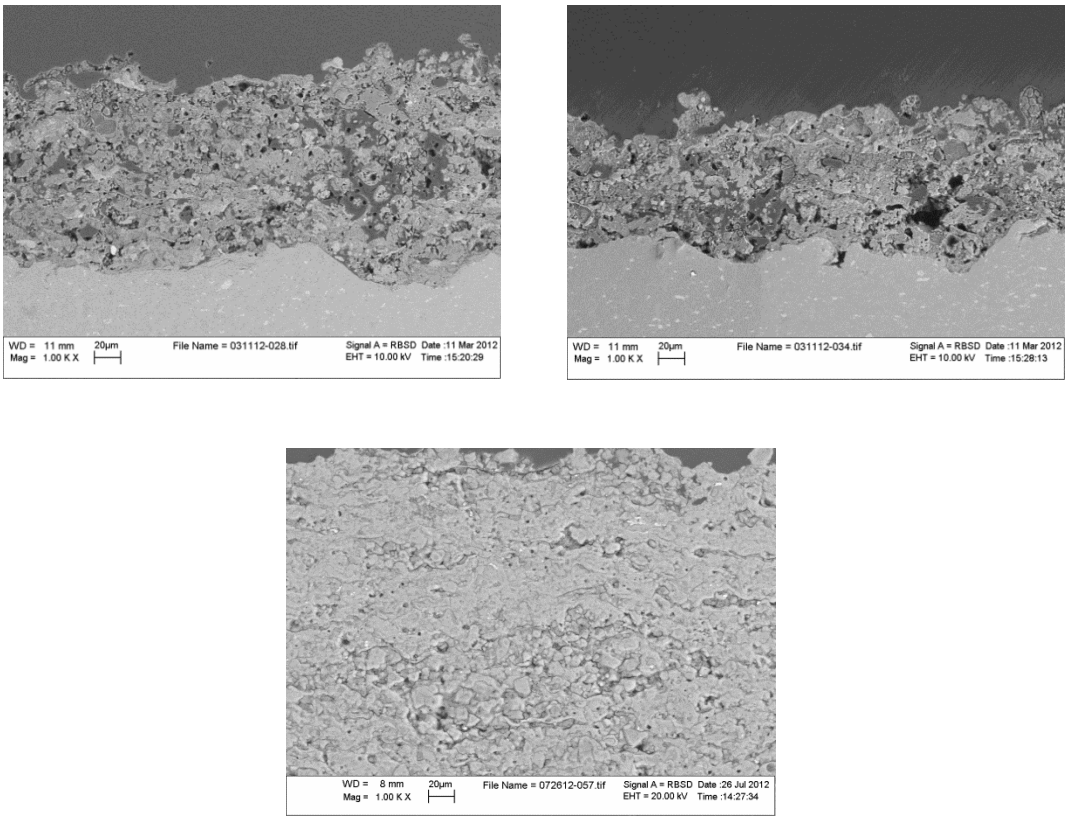

Figure 3-4. Cross-section of sample R1961, R1962, B006 (left, right, second line middle)

Figure 3-5 shows the cross-section of sample R1961, R1962 and B006 to study how different thermal spray parameters, such as temperature and velocity, affect the coating and influence different type of thermal spray torch on coating. These images were taken at same magnification and according to the images, there are no significant difference between sample R1961 and R1962, they are both porous with cracks and holes in the cross-section but it can be found that sample B006 has denser coating structure with less cracks. Further study of phase in sample B006 was carried out.

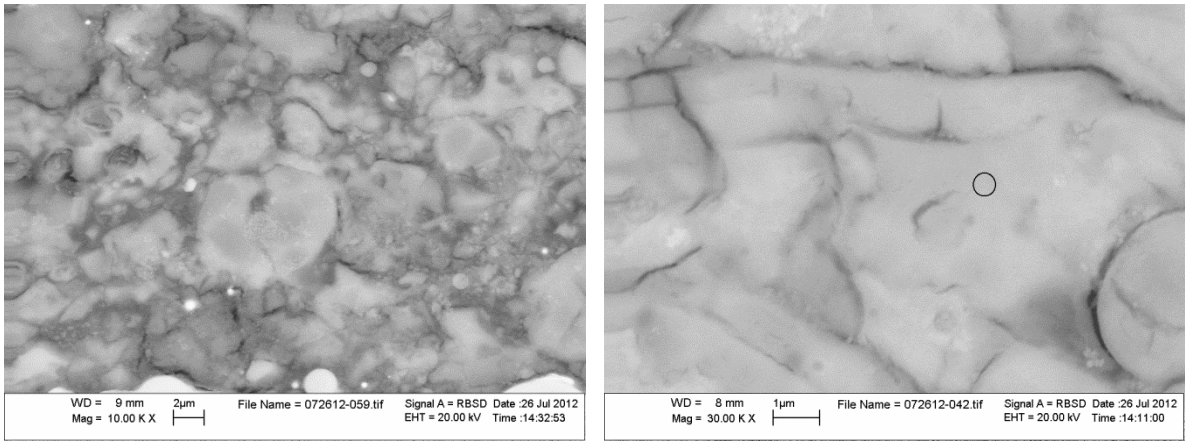

Figure 3-5. Cross-section of sample B006 with 30 kX mag

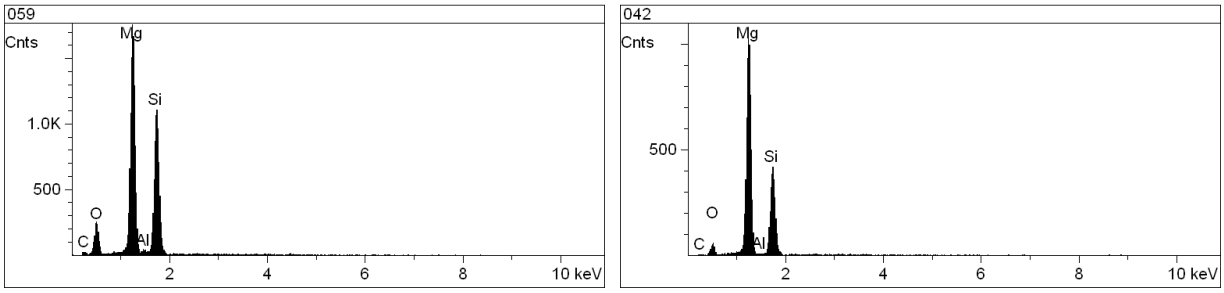

Figure 3-6. EDS of sample B006

With the help of EDS, the phase of sample B006 was clear that majority of phase in the cross-section are magnesium silicide because EDS can only examine the points instead of entire sample. In order to compare the composition of different samples, X-ray diffraction were used to make full comparison.

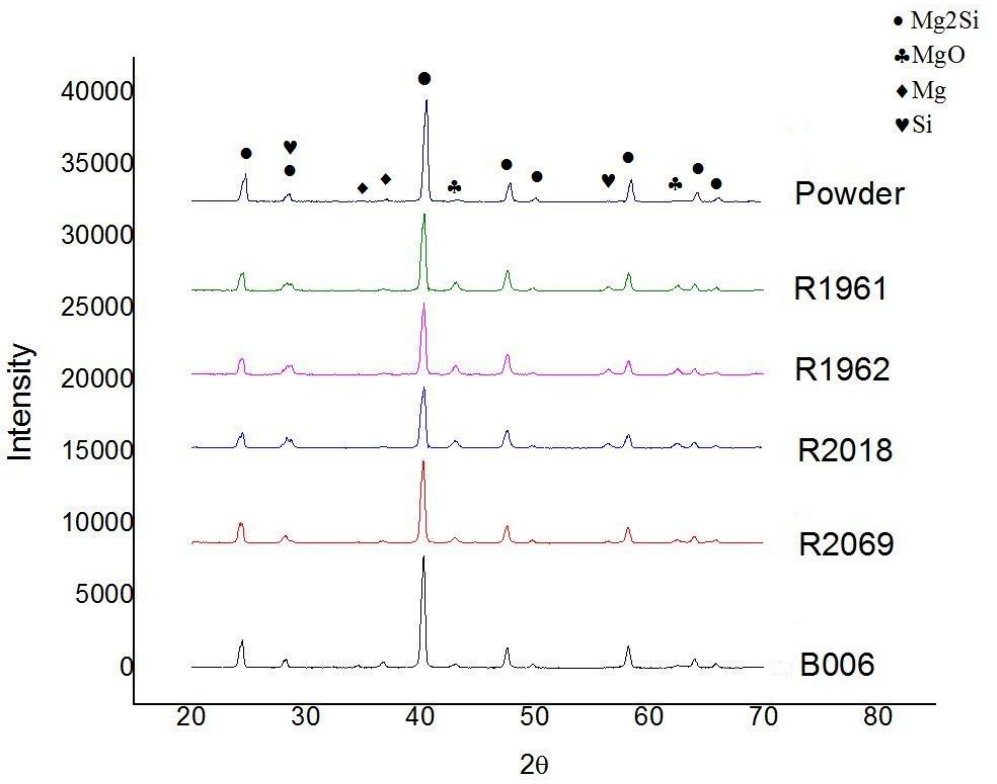

Figure 3-7. XRD of APS

In order to make a full comparison, the X-ray diffraction of raw powder was added into comparison so that any changes during the thermal process can be found. According to the graph above, sample B006 has the highest magnisium silicide concentration and lowest magnisium oxidize among all the APS samples; R1962 has lowest magnisium silicide concerntration and high magniusm oxides concerntration.

Table 3-2. Compositions of APS[24]

Sample	Mg_2Si, %	MgO, %	Si, %	Mg, %
Powder	98	1.3	-	0.4
R1961	77.5	17.0	5.5	-
R1962	76.0	16.7	7.3	-
R2018	78.6	14.9	6.5	-
R2069	86.0	10.4	3.6	+
B006	91.5	3.0	-	5.5

It can be seen that sample R2018 (with shroud) and R2096 (with smaller torch) increased the concerntration of magnisium silicide but at the same time, they decreased the concerntration of magnisium oxide; however, compare to sample B006, such increase in magnisium silicide and decrease in magnisium oxide are not significant. Since the scanning electron miscopy image were taken after X-ray diffraction analysis, sample R2018 and R2069 were not taken scanning electron miscopy images because X-ray diffraction already showed the oxidation rate of APS samples and the study of micro structure can reley on the study of sample B006 and R1961 or R1962 in that those two sample were made without shroud and smaller nozzle. The following thermal spray experiments were going to use same parameters with SG100 torch.

Comparison was made from these sample so that a conclusion was drown: sample B006 has highest magnisium silicide concerntration and lowest magnisium oxide concerntration, the

rest samples showed various concerntration of magnisium silicide, magnisium oxideand silicicon, none of them meet the desired concerntration as B006 achieved; therefore, a thicker layer of magnisium silicide coating were sprayed with same thermal spray parameters and SG 100 torch. The sample was named B015. Detail of thermal spray parameters are listed below:

Table 3-3. Thermal Parameters for sample B015

Plasma Gas	Argon
Current	450 A
Flow rate	105
Carrier Gas	Helium
Preheat times	4
Raster	500 mm/s
Pulse	2 s
Step	2mm
Powder feed rate	3.5 – 6rpm
Stand-off distance	100mm

At the same time, samples from hot-press method were also fabricated to serve as comparison.

Table 3-4. Hot-press parameters

Samples	Powder condition	Temperature(Celcius)	Pressure(MPa)
H1	98% Mg_2Si	800	30
H2	5% more Mg	800	30

Followed the same procedure, sample B015, H1 and H2 were analyzed by X-ray diffraction and scanning electron miscopy in the first place to examine the composition and micro-structure of the sample; However, samples should be polished before they go to scanning electron miscopy vacuum chamber.

Since all the coatings were sprayed on the titaniam plate or aluminium plate, the very first step was to peel off the metal plate and leave the coatings alone. The bonding between the coatings and metal substrate was rigid so that it cannot be simply peeled off. The typical way to do it was to use glue to attach the sample to a sample holder and leave the metal side out so that the metal can be polished; in detail, heated the glue till it was becoming the liquid and applied it onto the coating; and attached sample to the holder; then waited until the glue was cooled to the room temperature so the sample was strongly attached to the holder, even the friction from the polisher cannot take it off from holder. Then the metal plate was to polished on the polisher till as thin as possible. The sand paper was 60 mesh. Water was needed while polishing otherwise the heat that generated from the friction can melt the glue. It should take extremely attention

when the metal plate was polished thinner because the coating can easily be damaged by the polisher if the metal substrate was polished off.

When the metal substrate was thin, it can be peeled off from the coating by a small blade. After that, the glue can be washed off by actone. Furthermore, the coating itself is much softer then metal, so that sand paper can be switched to 400 mesh in order to polish the coating into desired shape. The techniques were the same as discussed before, use glue to attach the sample to the sample holder and polish.

For scanning electron miscopy purposes, the sample needs to be fixed into the mixture of resin and hardner. The mixture is a transparent solid when it dries and the ratio of resin and hardner was pre-determined and it can be looked up in the thermal spray laboratory. Note that the sample need to be placed into the vacuum chamber to vacuum because the mixture contains much air the it needs to be vacuumed out otherwise the mixture cannot be transparent when it dries, it will be full of bubbles.

The sample with mixture needs to be polished by various steps since the scanning electron miscopy requires the surface as flat as possible. The sand papers were used in the following order: 120 mesh, 240 mesh, 320 mesh, 400 mesh, 800 mesh, 1200 mesh and the sand disks was used in the following order: 3 micros, 1 micros and 0.5 micros. Note that when using the sand disks, the polishing liquids were also need to be sprayed on the sample to enhance the performace of the polishing.

The standard to examine the result was to check the reflection of the sample after using 1200 mesh sand paper. It shoud look like a mirror, highly reflective and no obvious scratches can be seen on the surface.

Scanning electron miscopy images of sample B015, H1 and H2 are presented below:

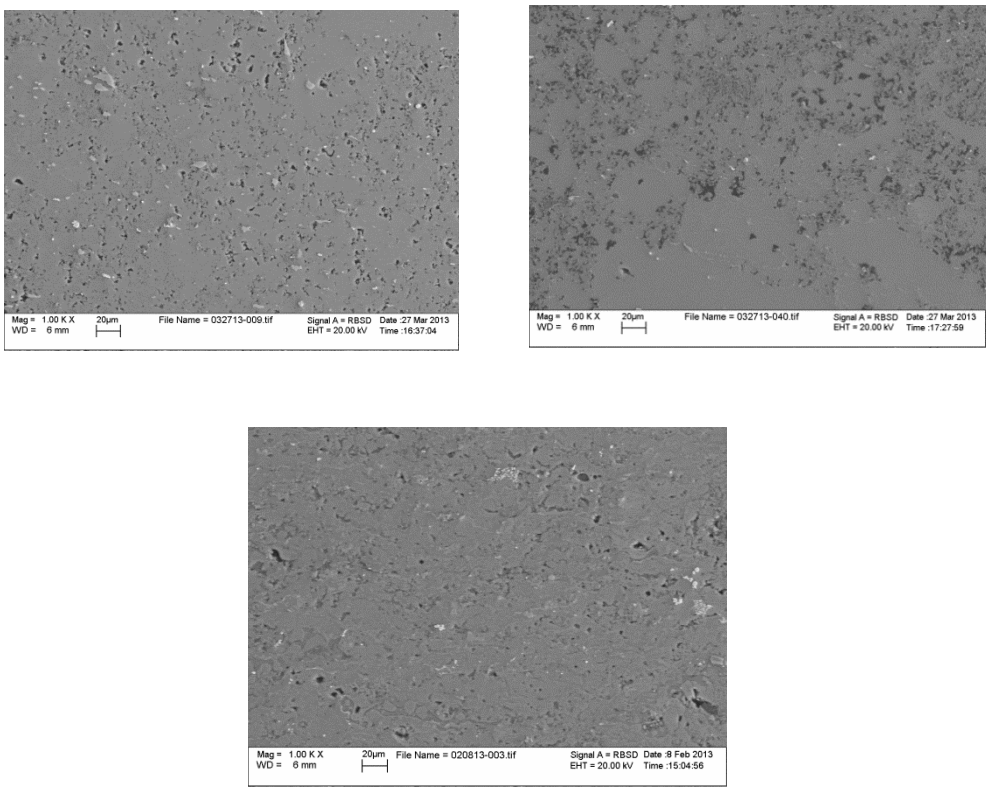

Figure 3-8. SEM images of sample H1, H2 and B015

Note that both sample H1 and H2 are from hot press method and H1 means magnisium silicide normal ratio in composition and H2 means the magnisium rich in composision; since the magnisium can easily be found in the APS sample B015 (according to Table 4, B015 shared the same thermal spray parameters as B006), by comparing these two hot press sample with manually Mg-rich , the influence of magnisium on the thermoelectrical properities can be discovered.

By analyzing the scanning electron miscopy images above, hot-press sample have less cracks than APS sample B015 even though there are pores in the cross-section. Impirities can be

seen as well. Further study of X-ray diffraction analysis can examine the concerntration of impurities.

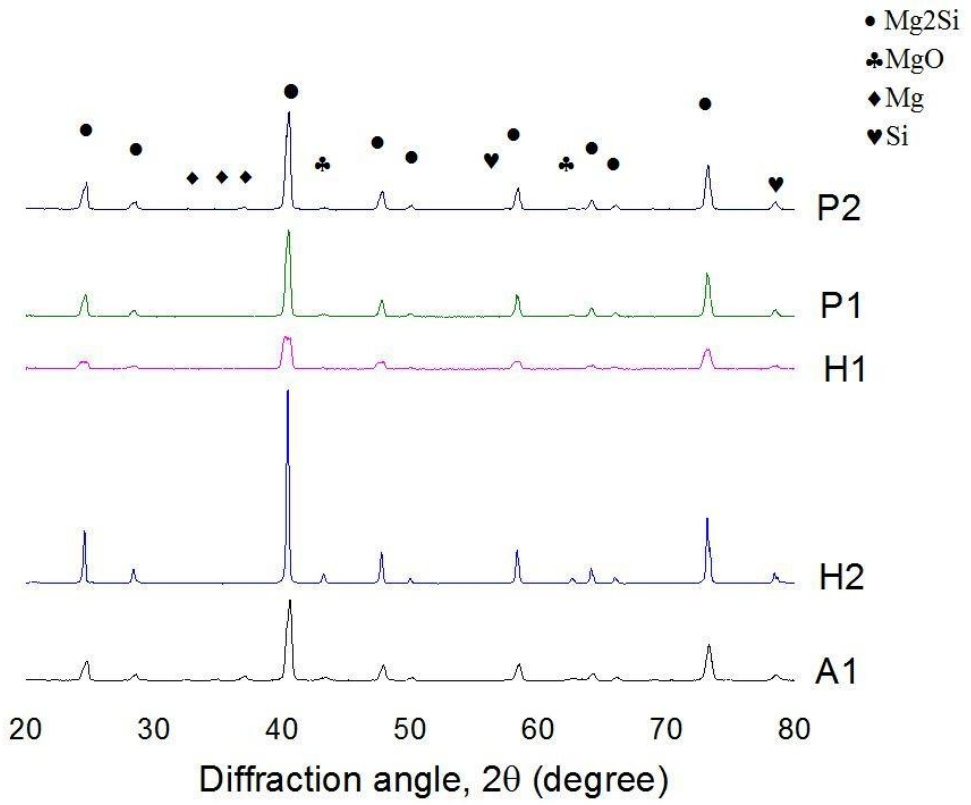

Figure 3-9. XRD of P2 (raw powder of normal ratio Mg_2Si), P1 (5% Mg rich powder), APS and hot pressed samples

From the figure of X-ray diffraction analysis, powder with Mg rich has more Mg peaks than normal ratio magnisium silicide powder so the raw powder before fabrication were in desired conditions. However, In hot press sample H1 and H2, there is no significant Mg peak; instead, Magnisium Oxide peaks were found during the analysis. The possible reason of such phnomena is the oxidation of Mg during the hot press since the whole manufacturing process were under atmospheric environment and remebmber that the reaction between magnisium and oxygen was active in the hot-press environment. Another explaination of absence of Mg peaks in hot press sample is that the volatilization of Mg during the hot press process. In the A1 curve

which is APS sample B015, Mg peak was found as expected and it may come from either raw powder or decomposition of magnisium silicide.

In conclusion, hot-press samples have less crack and pores than APS sample but they are not much denser than APS sample.

Before thermoelectric properties characterization, APS sample were annealed in order to reduce the amount of cracks and porous in order to see the influences on the thermoelectric properties. Related parameters are shown below:

Table 3-5. Annealing parameters for APS sample B015

Sample	Vacuum condition	Temperature(celcius)	Annealing time(hour)
A2	Vacuum	400	1
A3	Vacuum	400	20

20-hour annealing was undergone Hall Effect measurement before scanning electron miscopy since this sample was quantatively limited and it cannot be used after scanning electron miscopy image. The result showed that there was no any change in the mobility of electrons campared with 1-hour annealing; this means that 400 Celcius degree-20 hr annealing did not give any change to the thermoelectric properties. Scanning electron miscopy image was then taken with 1-hour annealed APS sample.

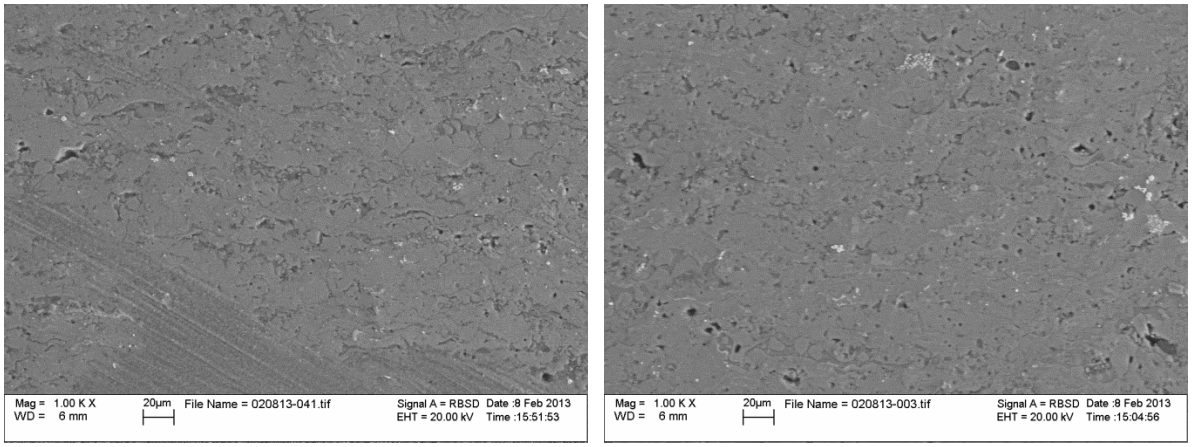

Figure 3-10. 1-hour 400 C annealed APS sample and APS without annealing

Comparing these two images, the first one is 1-hour 400 Celecius degree annealing APS sample, the second one is the APS sample withou annealing. It can be seen that there is no much change in the morphology of the cross-sections of thesee two samples. There are still cracks and pores distributed over the samples.Therefore, at this time, no solid conclusion of the influence of cracks and pores on thermoelectric properties can be drawn simply by scanning electron miscopy images. A possible explanation of it is that the temperature was not enough so there is no any changes on mobility between 1-hour and 20-hour annealing. Thermoelectric properties were then carried out.

3.1.2 Thermoelectric Properties of APS and Hot pressed samples

Thermoelectric properties include thermal conductivity, electrical conductivity and Seebeck Coefficient measurement. Hall Effect was also measured since it can explain the change of electrical conductivity.

Samples for thermal conductivity measurement needed to be prepared into cylinders with 0.5 inch in diameter and 1mm in height at most. At the same, the both surfaces of the sample need to be polished as flat as possible but not as good as those one for scanning electron miscopy images. The sample can be cut by laser so that a cylinder can be created. For electrical conductivity, since four points methods require flat surface, the sureface needs to be polished till it looks like a mirror. The size of it was 4 mm ×4 mm ×1mm at most, smaller was fine.

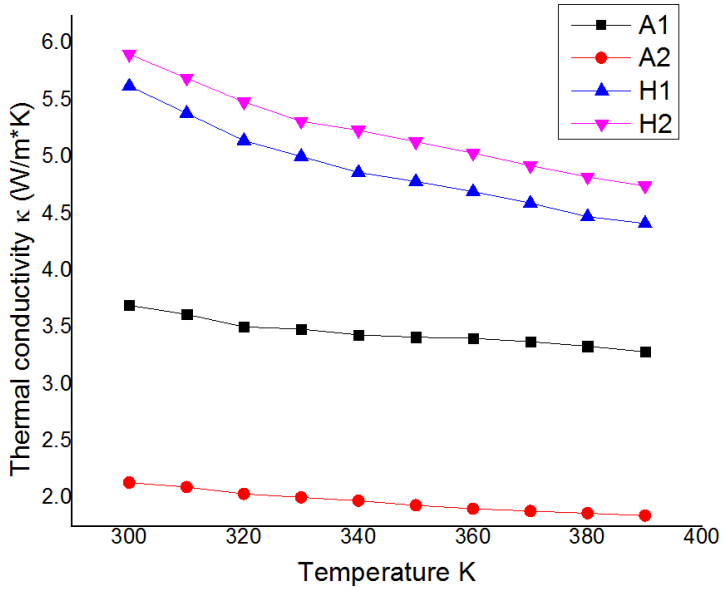

Figure 3.Thermal conductivity of APS samples and hot pressed samples

A1 is normal APS sample and A2 is annealed sample

Thermal conductivity measurement was taken from room temperature, 300K to high temperature, 390K. According to the figure above, the APS sample, both A1 and A2 fell into low thermal conductivity category while hot-press samples were in the high thermal conductivity category. In detail, annealed APS sample is even lower than normal APS sample and magnisium silicide normal hot-press sample has lower thermal conductivity than Mg rich hot-press sample.

According to the literature[25], cracks and pores in the APS samples contributes the scattering of phonons which is the heat carriers, so that the thermal conductivity can be lowered. In addition, electrons also carry heat so that the scattering of electron affects thermal conductivity. Note that annealed APS sample is even lower than normal APS sample, and at the same time, if the electrical conductivity of annealed sample is lower than normal APS sample, it can demostrate the statement that the electrons can also carry heat so electron scattering also affect the thermal conductivity. Moreover, by comparing the electrical conductivity of hot-pressed samples, one can determine the dominant factor for thermal conductivity.

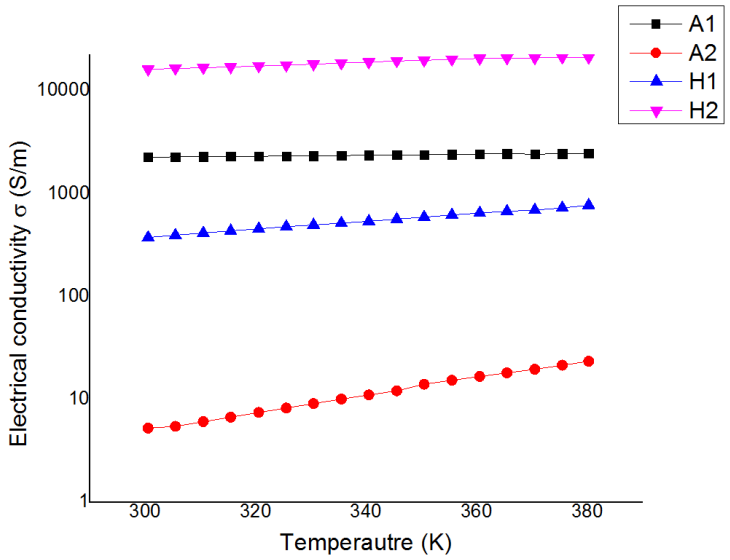

Figure 4-12. Electrical conductivity of APS sample and hot pressed samples

According to the figure above, the electrical conductivity of annealed APS sample has the lowest electrical conductivity which illustrates that the electrons were scattered so that the density of electrons was low, there were no too many electrons to transport heat; in all, thermal conductivity of annealed APS is low. So the dominant factor thermal conductivity is phonon scattering. It should also be noted that normal APS sample and both two hot-presses samples

have high elelctrical conductivity. To be specific, the 5% Mg rich hot-pressed sample has higher electrical conductivity than normal magnisium silicide ratio hot-presses sample is because of the metallic Mg in its composition; however, normal APS sample also showed high electrical conductivity which is hard to explain solely from micro-structure and electrical and thermal conductivity measurement. Thus, Hall Effect was measured.

Hall Effect measurement can render carrier concerntration and mobility of a certain material by mearueing Hall Coefficient R_H; it is defined as:

$$R_H = -\frac{1}{ne}$$

The electrical conductivity can be defined by the following equation:

$$\sigma = n \cdot e \cdot \mu$$

where σ is the electrical conductivity; n is carrier concentration; e is electron charge and μ is the mobility of carrier.

Table 3-6. Hall Effect measurement of APS samples and hot pressed samples[26]

Sample	Carrier concerntration ($10^{17}/cm^3$)	Mobility ($cm^2/V•s$)	Conductivity (S/m)
A1	4270	0.15	1025
A2	8.26	0.51	6.7
H1	22.6	13.3	481
H2	258	26.7	11025

Note that A1 and A2 are APS samples and H1 and H2 are hot pressed samples. Variation of electrical conductivity may be caused by noise during the measurement but all the data fall into the desired trend. Combining the table and the equation of definition of elecrtrical conductivity, carrier concerntration and mobility determine the electrical conductivity and it can easily be seen that, all four samples fit the trend of the calculation so the high electrical conductivity APS sample can be explained as the high carrier concerntration even though the relatively low mobility.

It is interesting that both two hot-pressed samples have much higher carrier mobility than thermal sprayed samples and the carrier concerntration is at same level. It is known that contamination, impurities and grain boundries in the sample can influence the carrier mobility. According to existing data and scanning electron miscopy images, the scanning electron miscopy images of APS samples have white particles which are impurities existing in both normal APS sample and annealed sample, but it is hard to find in the hot-pressed samples. Nevertheless,

scanning electron miscopy images were taken at certain areas instead of whole cross-section, such characterization technique cannot demonstrate the percentage of impurities in the composition; therefore, it is hard to determine how much influence of impurities on the carrier mobility.

Grain boundries in the thermal sprayed sample are hard to test since thermal spray coatings of magnisium silicide was highly disordered. The more grain boundries, the less mobility will be since the mobility is dominated by electron scattering, grain boundries can affect the travel of electrons so the carrier mobility is low for high grain boundries material. Same to cracks and pores, they serve the same purpose as grain boundries.

The annealed APS sample has high carrier mobility than normal APS sample is because the annealing reduce the amount of grain boundries. The effect was not significant, and it was because of the low annealing temperature. It can be raised up to high temperature in vacuum condition to further examine the effect of annealing on thermoelectric properties.

The Seebeck Coefficient of the APS samples and hot pressed samples were measured as shown in figure below:

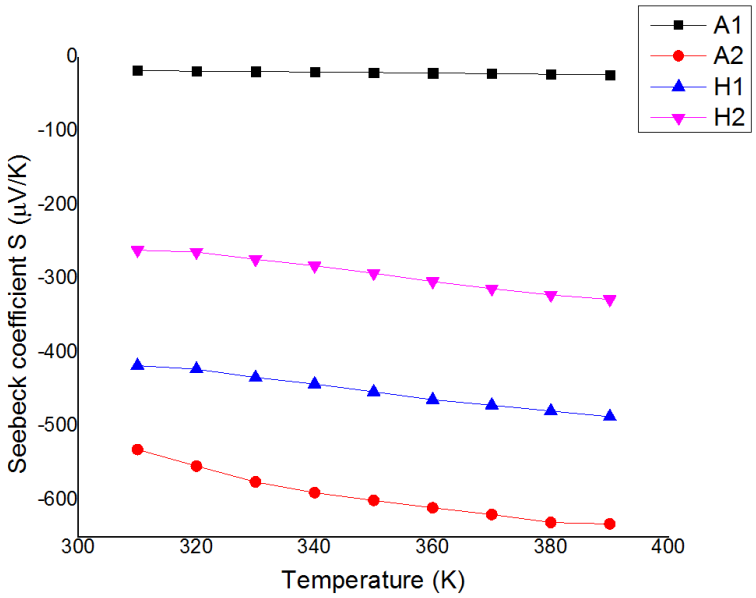

Figure 5. Seebeck Coefficient of Aps and hot pressed samples

The equation of Seebeck Coefficient can be defined as follow[27]:

$$S = -\frac{k}{e}\left(\frac{5}{2} + r + \frac{lnN_c}{n}\right)$$

Where S is Seebeck Coefficient; k is Boltzman constant; r is exponent of power function of energy-dependent relaxation time expression; N_C is effective density of state of valence band; n is the carrier concerntration. Based on the equation above, the Seebeck Coefficient is inversely propotional to the carrier concerntration, so as to electrical conductivity.

Combining figure 3-13 and table 7, annealed APS sample has the lowest corrier concerntration so the seebeck of annealed APS sample has the highest absolute value; normal APS sample has the highest carrier concerntration wich result in the lowest seebeck absolute value. Hot-pressed sample were in the middle range according the respective carrier concerntration.

Seebeck Coefficient is not directly affected by the micro-structure[28] but more rely on the phase composition. In this study, magnisium silicide was not doped and was used as n-type semiconductor. The more magnisium silicide concerntration in the composition, the higher seebeck coefficient it can reach and carrier concerntration is related to magnisium silicide because magnisium silicide is the thermoelectric material. During the annealing, the small amount of Mg left in the sample reacted with the small portion of oxygen in the vacuum chamber or, evaporized; Mg is an active mateiral, it increases the electrical conductivity, so that the decrease of total concerntration of Mg may increase the carrier concerntration. Comparing the two hot-pressed samples, the one with higher Mg concerntration has lower seebeck coefficient, wich further explain the effect of Mg concerntration on the Seebeck Coeffcient.

The figure of merit (ZT) of these four sample were also calculates and ploted.

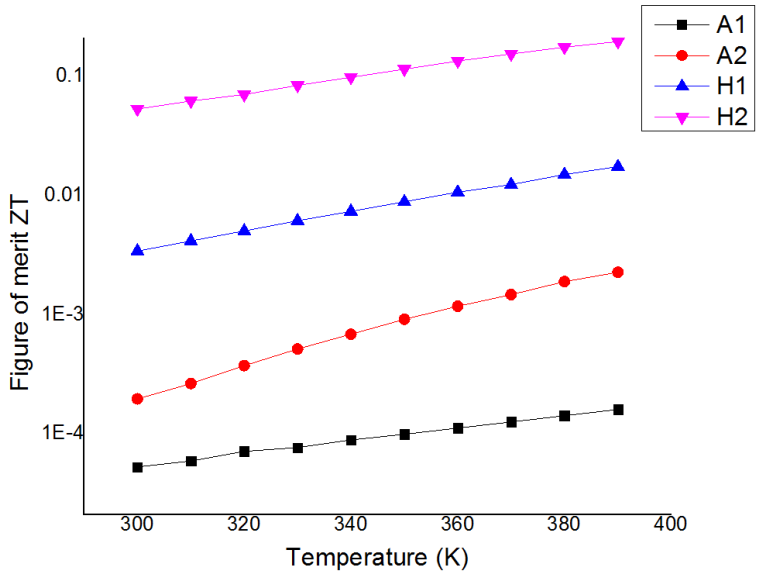

Figure 6-14. Figure of merit of APS and hot pressed samples

The equation[29] of such calculation is given by:

$$\mathrm{ZT} = \frac{\sigma S^2 T}{k}$$

Note that σ is electrical conductivity; S is seebeck Coefficient; T is the temperature and k is the thermal conductivity.

Among these four materials, 5% Mg rich hot-pressed sample had the largest figure of merit , followed by normal ratio hot-pressed sample. Thermal sprayed sample A1 and annealed thermal sprayed sample were the lower than hot-pressed sample and annealed sample was higher than the other one. ZT cannot be determined by single parameter, it is the result of all three thermoelectric properties. Thus, both of them had much higher thermal conductivity, but Mg rich hot-pressed sample had the highest electrical conductivity; the seebeck was lower than APS samples but it did not affect the overall ZT. Followed by normal ratio hot-pressed sample, it had high electrical conductivity and high seebeck coefficient. APS sample with annealing was low in ZT because of the low electrical conductivity, although it had the highest absolute seebeck coefficient and lowest thermal conductivity.

3.2 Vacuum Plasma Spray

Vacuum plasma spray was also carried out to make magnesium silicide coatings. The powder was same as used for Atmospheric plasma spray. Magnesium silicide powder was deposited on the aluminum substrates and the size of the substrates was same as the one that used for Atmospheric plasma spray

In order to find out the optimal parameters for vacuum plasma spray, multiple samples were made. The main difference was the different power supply. The samples were compared with hot-press samples and they are listed below:

Table 3-7. Sample comparison with hot pressed samples;

Sample name	Synthesis cond.	Condition	Powder cond.
V1	VPS	18kw	Normal ratio
V2	VPS	18kw	Mg rich
V3	VPS	21kw	Normal ratio
H1	HP	800 ºC, 30MPa	Normal ratio
H2	HP	800 ºC, 30MPa	Mg rich

3.2.2 SEM and XRD Analysis of VPS and Hot pressed samples

Characterization was done by the following process: X-ray diffraction, scanning electron miscopy, thermal conductivity, electrical conductivity and Seebeck Coefficient.

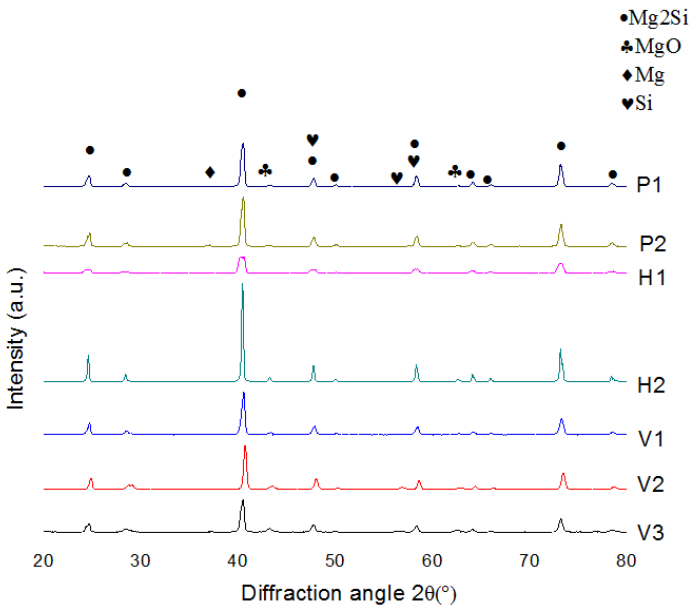

Figure 7. XRD analysis of VPS samples, HP sample and raw powder.P1 is normal Mg powder; P2 is Mg rich powder

Remember that the reaction between magnesium silicide and oxygen is 450 ^{o}C but the temperature on the deposited surface is much higher than this temperature; however, vacuum plasma spray was conducted in vacuum condition; so the reality was that the vacuum chamber was not absolutely vacuum but still it provided a significant low pressure in the chamber which can be seen as non-oxygen condition. It decreased the total amount of oxidation of magnesium silicide.

By analyzing the X-ray diffraction result, the MgO peak and Si peak are fairly consistent with the raw powder and but still, there is observable variation happened on the V3 sample, which is 21kw normal Mg VPS sample. This is because the higher power applied to the thermal spray gun and the reaction of oxidation and decomposition of magnesium silicide. V1 and V2 are normal Mg VPS sample and Mg rich sample respectively but they did not show any

significant change in composition. H1 and H2 are hot pressed samples. Same as Atmospheric Plasma Spray, H2 appeared higher MgO peak compared to the H1 and this is because H2 is Mg enriched sample and the reaction of Mg and oxygen that made the MgO peak.

Scanning electron miscopy images can observe the cross-section of the VPS sample so that it can help understand the thermal conductivity and electrical conductivity in a physical way.

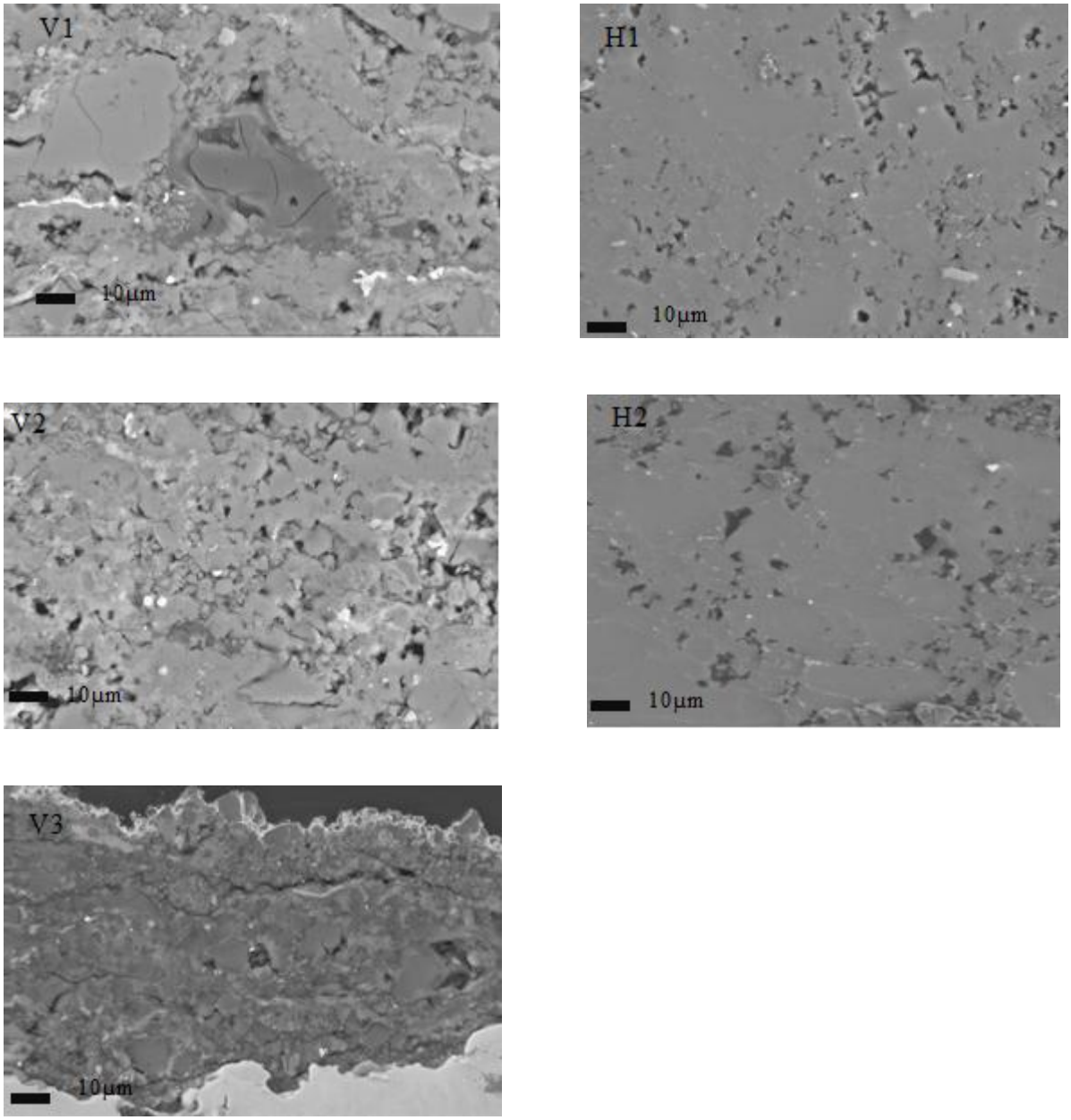

Figure 3-16. SEM images of VPS sample and hot pressed samples

Images V1, V2 and V3 are VPS sample images, compared to the HP images on the right (H1 and H2), they have more cracks and pores and this is due to the poor melting conditions during the thermal spray. V3 has less cracks and pores than the other two samples since V3 was

fabricated in 21kw power supply so the powder was better melted. The overall result was within expectation because vacuum plasma spray does not have as good melting condition as atmospheric plasma spray.

3.2.2 Thermoelectric properties of VPS and Hot pressed samples

The thermal conductivity and electrical conductivity are high related to the micro-structures since the cracks and pores may block the heat transfer and electron transfer. The more uniform structure, the higher value of conductivity it can present. The following image shows the thermal conductivity of VPS sample and hot press samples.

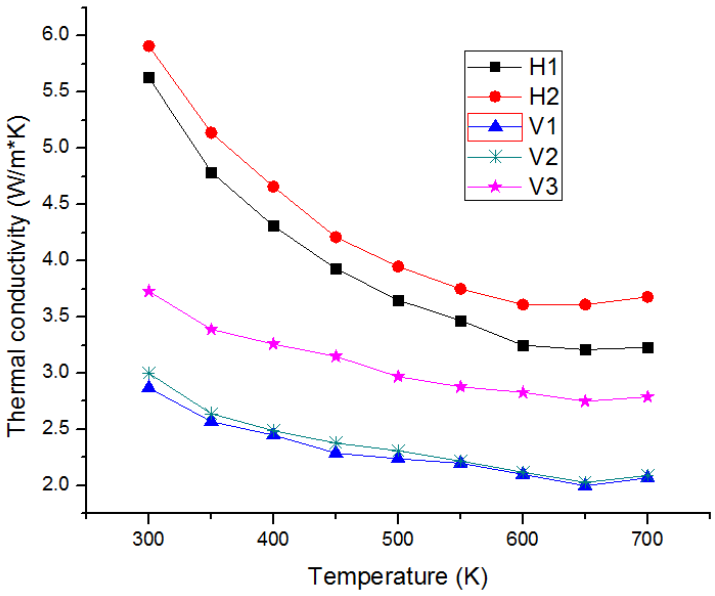

Figure 8. Thermal conductivity of VPS samples and hot pressed samples

The temperature was measured from room temperature to 700K for VPS and hot pressed samples. According to the graph, all the three VPS samples have lower thermal conductivity values because the numbers of cracks and pores that exist in the samples are more than in the hot

pressed samples. Among the VPS samples, V1 and V2 were made from 18kw power supply, which is lower than 21kw, so that melting condition is worse than the 21kw sample; therefore, both of the two 18kw samples have less thermal conductivity than the 21kw sample. The difference between the two 18kw samples is the Mg content. V2 is Mg rich sample. It can be seen that V2 has little higher thermal conductivity but not significantly higher. It cannot be explained simply by the scanning electron miscopy images. It is likely due to the electron concentration in the sample which will be discussed in the next section.

Hall Effect and electrical conductivity were measured. They are highly correlated because of the equation $\sigma = ne\mu$, where σ is electrical conductivity, n is carrier concentration, e is charge and μ is the mobility of electrons. The Hall Effect result is listed below:

Table 3-8. Hall Effect measurement of VPS and HP samples

Sample	Carrier concentration, n, (10^{17}/cm^3)	Mobility, μ, (cm^2/V•s)	Conductivity, σ (S/m)
H1	22.6	13.31	481
H2	258	26.72	11040
V1	8.24	1.31	17.3
V2	10.5	1.74	29.3
V3	7.94	3.14	40

Hall Effect was measured under room temperature so it varied as the temperature went up but due to the limitation of the equipment, high temperature Hall Effect could not be measured. The result of electrical conductivity is as follow:

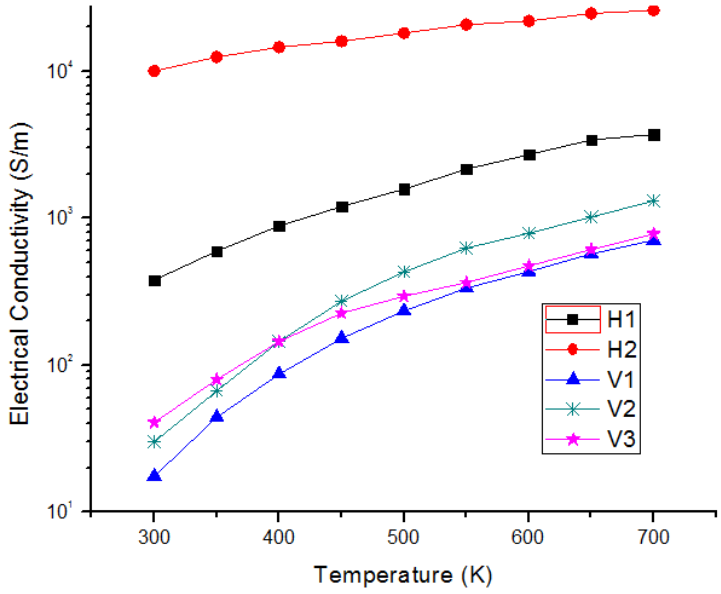

Figure 9-18. Electrical conductivity of VPS and hot pressed samples

Combining the Hall Effect measurement and electrical conductivity measurement, it fits perfectly in the room temperature, the values of electrical conductivity of VPS and HP samples were in the order. However, they varied as the temperature went up. V2 became the highest one among all three VPS samples and this is Mg rich sample. Thus, the Mg concentration contributes the high electrical conductivity. Same as H2 sample, H2 is Mg rich hot pressed sample and due to its high mobility, it has the highest electrical conductivity among all the samples. Followed by the same theory, higher mobility can render higher electrical conductivity and it can be further demonstrated by samples V1 and V3. Remember that V1 is 18kw normal Mg ratio VPS sample and V3 is 21kw normal Mg ratio VPS sample and the electrical conductivity of V3 is higher than V1 in that 21kw power supply had a better melting condition during the fabrication than 18kw

power supply; better melting condition mean the denser micro-structure so V3 has higher mobility.

The mobility is also affected by the impurities in the samples. They can come from the raw samples or from the fabrication process and they had been detected in the VPS samples with scanning electron miscopy and EDX. At the same time, mobility at high temperature is determined by phonon scattering[30]. More impurities will result in more strong electron scattering and further result in a decreased mobility.

Seebeck Coefficient was measured from room temperature to high temperature, 700 K since 700K is more approached to the real working temperature of vehicle exhaust pipe. The result is shown as follow:

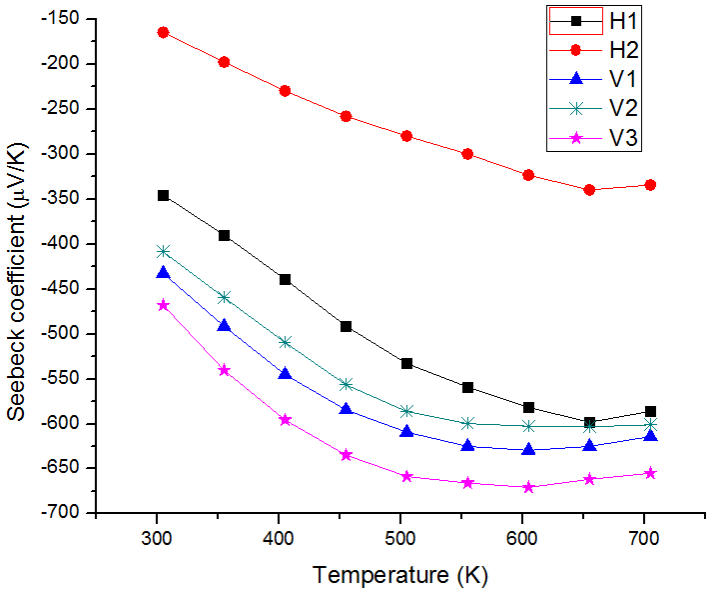

Figure 10-19. Seebeck Coefficient of VPS and hot pressed samples

According to literature, Seebeck Coefficient is not affected by the micro-structure but depends on the phase composition[28]. In addition, an equation, shown as follow also illustrates the parameters that affect the overall Seebeck Coefficient.

$$S = -\frac{k}{e}\left(\frac{5}{2} + r + \frac{lnN_c}{n}\right)$$

Remember that k is Boltzmann constant, e is electron charge, r is exponent of power function of energy-dependent relaxation time expression; N_C is effective density of state of valence band; n is the carrier concerntration. Since n is inversely proportional to electrical conductivity, data from Table 10 can validate the correctieness of the equation. By analyzing all the samples, it can be found out that the concerntration of Mg can increase the carrier concerntration but decerease the Seebeck Coefficient. Both H2 and V2 can demonstrate this point at hot pressed catogory and VPS catogory; All the hot pressed samples have much higher carrier concerntration than VPS samples so they all have less Seebeck Coefficient.

The figure of merit is defined as

$$ZT = \frac{\sigma S^2 T}{k}$$

ZT is figure of merit, σ is electrical conductivity, S stands for Seebeck Coefficient and k is thermal conductivity. Combining the tables above regarding on VPS samples, the figure of merit can be calculated and listed as following graph:

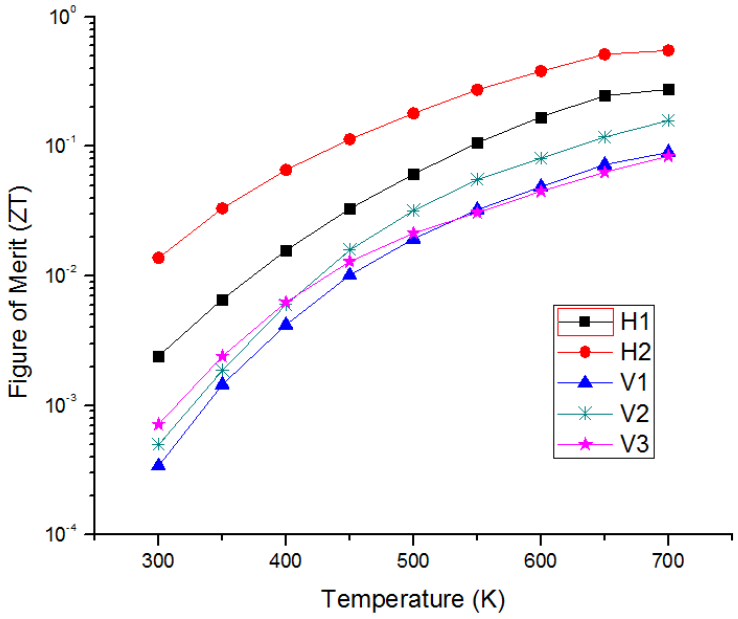

Figure 11-20. Figure of merit of VPS and hot pressed samples

The values of VPS samples are lower than hot pressed samples and this is due to the tradeoff of thermal conductivity and electrical conductivity. The sample which has a promising figure of merit is V2, the 18kw Mg-rich VPS sample because at 700 K, it reaches 0.1; this is increase of figure of merit can be treated as doping, Mg is the doping element in the sample and an assumption is that the proper doping as further increase the figure of merit. The overall VPS samples are getting close to 0.1 at 700K. Compared to hot pressed sample, VPs samples have lower figure of merit in that electron mobility plays a key role in this equation and as to thermal sprayed samples, the mobility is not as good as hot pressed samples.

Chapter 4

Conclusions and Future work

4.1 Conclusions

Magnesium silicide was fabricated by thermal spray in atmospheric plasma spray and vacuum plasma spray. Scanning electron microscopy images were taken in order to examine the micro-structure; X-ray diffraction was taken to analyze the composition of the sample which is important to the work. Thermal conductivity, electrical conductivity and Seebeck coefficient were measured so that the figure of merit can be evaluated. In addition, Hall Effect was measured as well because it can provide a way to evaluate the electrical conductivity and explain the decrease of thermal conductivity.

In all, Atmospheric Plasma Spray and Vacuum Plasma Spray just stand for two different spraying methods that can be used in the thermal spray. The overall result from Vacuum Plasma Spray has better performance in figure of merit and in addition, it is known that the figure of merit comes from the combination of thermal conductivity, electrical conductivity and Seebeck Coefficient. Thus, to be more specific, the best thermal conductivity of VPS sample is on the same level as APS sample within the range of room temperature to 700K; electrical conductivity of VPS is higher than APS and the Seebeck Coefficient of VPS is at same level with APS as well.

Meanwhile, the mobility of the carriers can be enhanced by reducing the total amount of grain boundaries and impurities. The impurities may come from the raw powder or fabrication process. By increasing the mobility, the electrical conductivity can be increases of the basis of same carrier concentration. The thermal conductivity can be decreased by increasing pores and cracks in that those two factors contribute the phonons scatterings; but at the same time, they can decrease the electrical conductivity.

For the Seebeck Coefficient, it is not dependable on the micro-structure; instead, it depends on its composition. If the ratio of Mg_2Si is higher, the Seebeck Coefficient should be higher.

However, a solid conclusion of which method is better for synthesis magnesium silicide cannot be drown yet because all the samples we made are small scale and for VPS samples, there are still more work left undo and this will be discussed in the next section.

4.2 Future Work

Even though a variety of works had been done for both VPS and APS, there are still more works can be extended according to our result.

As to the APS method, large-scale fabrication can be tried. Eventually the device will be in an integrated cylindrical shape, which means that the powder will be sprayed on a curved surface; so the mechanical bonding between the coating and surface needs to be tough and strong. Moreover, Mg enriched powder was also used in the APS work and Mg can be treated as doping element; however, Mg is not the only doping element, elements such as Bi, Ag, etc. can be used

as well; then to measure the high temperature properties because we knew from our previous result that the properties could be changed when the temperature increases.

As to the VPS method, annealing can be tried. Noted that the VPS samples were fabricated in the vacuum condition, annealing needs to be done in a vacuum chamber that should not be worse than that used for fabrication otherwise samples will be oxidized in the chamber. Still, annealing parameters need to be adjusted; this work requires trials and errors. In addition, just like APS sample, other doping elements can also be tried. One thing needs to be noted is that VPS does not provide good melting condition, which is important to the mechanical bonding of the coating; if the bonding is not as hard enough, the coating might be peeled off from the cylinder.

Furthermore, the device is not the only consists of magnesium silicide coating, it also requires the other types of semiconductor materials and it needs to be found and thermal sprayed onto the cylinder so that the whole device can be made.

Reference

1. Yang, J. and F.R. Stabler, *Automotive Applications of Thermoelectric Materials.* Journal of Electronic Materials, 2009. **38**(7): p. 1245-1251.
2. Bell, L.E., *Cooling, Heating, Generating Power and Recovering Waste Heat with Thermoelectric System.* Science, 2008. **321**.
3. Donghong Wei, X.L., Zhen Lu, Jianming Gu, *Performance analysis and optimization of organic Rankine cycle (ORC) for waste heat recovery.* Energy Conversion and Management, 2007. **48**(4): p. 1113-1119.
4. Inc.), U.H.C., *Diesel Engine Waste Heat Recovery Utilizing Electric Turbocompound Technology*, in *2004 DEER Conference*. 2004.
5. Patel, P., *Powering Your Car with Waste Heat*, in *MIT Technology Review*. 2011.
6. André, C., et al., *Extruded Bismuth-Telluride-Based n-Type Alloys for Waste Heat Thermoelectric Recovery Applications.* Journal of Electronic Materials, 2009. **38**(7): p. 1061-1067.
7. S. Choi, K.K., W. Seo, *Synthesis, Characteristics and Thermoelectric Properties of the Rare-earth-doped Mg2Si System.* J. Korean Phys. Soc. **57**.
8. Zhang, Q., et al., *Thermoelectric performance of Mg2−xCaxSi compounds.* Journal of Alloys and Compounds, 2008. **464**(1-2): p. 9-12.
9. Hou, Q.R., et al., *Thermoelectric properties of p-type higher manganese silicide films prepared by solid phase reaction and reactive deposition.* physica status solidi (a), 2007. **204**(10): p. 3429-3437.
10. IKUTO, A., *Doping Effects on Thermoelectric Properties of Higher Manganese Silicides (HMSs, MnSi1.74) and Characterization of Thermoelectric Generating Module using p-Type (Al, Ge and Mo)-doped HMSs and n-Type Mg2Si0.4Sn0.6 Legs.* Japan Journal Application Physics, 2005. **44**(6): p. 4275-4281.
11. Strasser, M., et al., *Miniaturized thermoelectric generators based on poly-Si and poly-SiGe surface micromachining.* Sensors and Actuators A: Physical, 2002. **97-98**: p. 535-542.
12. Li Shi, J.G., Matt Hall, Jianshi Zhou, *High-Performance Thermoelectric Devices Based on Abundant Silicide Materials for Vehicle Waste Heat Recovery*, in *2011 Thermoelectrics Applications Workshop*. 2011.
13. J. LaGrandeur, D.C., S. Hung, B. Mazar, and A. Eder, *Automotive Waste Heat Conversion to Electric Power using Skutterudite, TAGS, PbTe and BiTe*, in *25th International Conference on Thermoelectrics*. 2006.
14. Zaitsev, V., et al., *Highly effective Mg2Si1−xSnx thermoelectrics.* Physical Review B, 2006. **74**(4).
15. Riffel, M. and J. Schilz, Journal of Materials Science, 1998. **33**(13): p. 3427-3431.

16. Jung, J.-Y. and I.-H. Kim, *Synthesis and Thermoelectric Properties of n-Type Mg2Si.* Electronic Materials Letters, 2010. **6**(4): p. 187-191.
17. Li, Q., Z. Lin, and J. Zhou, *Thermoelectric Materials with Potential High Power Factors for Electricity Generation.* Journal of Electronic Materials, 2009. **38**(7): p. 1268-1272.
18. Sampath, S., *Thermal Spray Applications in Electronics and Sensors: Past, Present, and Future.* Journal of Thermal Spray Technology, 2010. **19**(5): p. 921-949.
19. Metco, S., *An Introduction to Thermal Spary.*
20. Instruments, T., *Principan Methods of Thermal Conductivity Measurement.*
21. *Jandel Multiheight Probe Instructions.*
22. F.M.Smith, *Measurement of Sheet Resisitivities with the Four-Point Probe.* The Bell System Technical Jounal, 1958. **37**: p. 711-718.
23. Technologies, M., *Seebeck Effect Software MMR-Tech.*
24. Gaosheng Fu, Lei Zuo., Jon Longtin, Yikai Chen, Sanjay Sampath, *Progress on searching optimal thermal spray parameters for magnesium silicide*, in *Materials Research Society*. 2013: Boston.
25. Chi, W.G., S.Sampath, and H.Wang,, *Microstructure-thermal conductivity relationships for plasma-sprayed yttria-stabilized zirconia coatings.* Journal of the American Ceramic Society, 2008: p. 2636-2645.
26. Gaosheng Fu, Lei Zuo., Jon Longtin, Chao Nie, Yikai Chen, Mahder Tewolde and Sanjay Sampath, *Thermoelectric Properties of Magnesium Silicide Deposited using Atmospheric Plasma Thermal Spray* Journal of Electronic Materials, 2013.
27. Busch, G.a.U.W., *Elektrische Leitfahigkeit Und Hall-Effekt Intermetallischer Verbindungen.* Helvetica Physica Acta, 1953. **36**(3-4): p. 395-399.
28. Hu, Y.F., et al., *Thermoelectric properties and microstructure of c-axis-oriented Ca3Co4O9 thin films on glass substrates.* Applied Physics Letters, 2005. **87**(17).
29. Min, G., D.M. Rowe, and K.Kontostavlakis, *Thermoelectric figure-of-merit under large temperature differences.* Journal of Physics D-Applied Physics, 2004. **37**(8): p. 1301-1304.
30. Arora, N.D.H., J. R. Roulston, D. J., *Electron and hole mobilities in silicon as a function of concentration and temperature.* IEEE transaction on Electron Devices, 1982. **29**(2): p. 292-295.